Synthesis of Tricyclic 1,3-Oxazin-4-ones and Kinetic Analysis of Cholesterol Esterase and Acetylcholinesterase Inhibition

Markus Pietsch and Michael Gütschow*

Pharmaceutical Institute, University of Bonn, Kreuzbergweg 26, D-53115 Bonn, Germany

Received August 31, 2005

A series of thieno[1,3]oxazin-4-ones and thieno[1,3]thiazin-4-ones were synthesized and investigated as inhibitors of the α/β hydrolases cholesterol esterase (CEase) and acetylcholinesterase (AChE). The introduction of a cycloaliphatic five- or six-membered ring fused at the thiophene was favorable for CEase inhibition. Such compounds were analyzed as true alternate substrate inhibitors. 6,7-Dihydro-2-(dimethylamino)-4*H*,5*H*-cyclopenta[4,5]thieno-[2,3-*d*][1,3]oxazin-4-one (**33**) exhibited a K_i value of 630 nM and excelled in its low susceptibility to CEase-catalyzed degradation. Compound **33** and its analogues did not inhibit AChE. The introduction of a tetrahydropyrido ring with bulky hydrophobic substituents at the basic nitrogen provided inhibitors of AChE which were completely inactive toward CEase. 7-Benzyl-5,6,7,8-tetrahydro-2-(*N*-3,4-dimethoxybenzyl-*N*-methylamino)-4*H*-pyrido[4′,3′:4,5]thieno[2,3-*d*]-[1,3]oxazin-4-one (**21**) had the IC_{50} value of 330 nM for AChE inhibition. A residual enzymatic activity at an infinite inhibitor concentration and thus a catalytically active ternary enzyme−substrate−inhibitor complex was concluded. To specify kinetic parameters of inhibition, a new method was derived to characterize selected thieno[1,3]oxazin-4-ones as hyperbolic mixed-type inhibitors of AChE.

Introduction

Cholesterol esterase (CEase, EC 3.1.1.13) and acetylcholinesterase (AChE, EC 3.1.1.7) belong to the α/β hydrolase family.[1,2] This protein family is characterized by the α/β hydrolase fold, a structural motive consisting of a mostly parallel, eight-stranded β sheet surrounded on both sides by α helices. Although their members are related by divergent evolution, the α/β hydrolase fold is able to provide a stable scaffold with spatial positions for the active site components, that are well conserved in all enzymes of the family.[2−5] CEase and AChE contain a catalytic triad composed of serine, histidine and an acidic amino acid (CEase: Asp, AChE: Glu), that are positioned in very short loops beyond the end of strands five, eight and seven, respectively.[1,3] Like serine proteases, CEase and AChE utilize an acylation−deacylation mechanism. Both the acylation and deacylation stages transit tetrahedral intermediates that are stabilized by a bi- or tripartite oxyanion hole.[1,3,4,6,7] While there are similarities in the tertiary structure and the catalytic mechanism, CEase and AChE differ in the substrate specificity as well as in their physiological functions and their role in pathological processes.

The three-dimensional architecture of CEase is known from several crystal structures.[8−11] CEase is a less specific lipolytic enzyme. The activation by primary bile salts is required for the hydrolysis of a broad spectrum of substrates, including lipophilic compounds with long-chain fatty acid moieties such as cholesterol esters, triacylglycerols, phospholipids, and ceramides.[12−16] The hydrolysis of water-soluble substrates such as esters of short-chain fatty acids or lysophospholipids is not strongly dependent on bile salt activation.[16] CEase mainly originated from pancreatic acinar cells and lactating glands of higher mammals and released into the circulation was also found in the liver, in macrophages, endothelial cells, and eosinophiles.[16] Once secreted into the lumen of the duodenum, pancreatic CEase, together with other pancreatic lipolytic enzymes and preduodenal lipase, acts to complete the digestion of dietary lipids.[12,13]

On the basis of a proposed model, CEase has a dual effect on cholesterol absorption by virtue of both the hydrolysis of dietary cholesterol esters and lecithin. Thus, CEase contributes to the formation of lysolecithin-rich micelles, which act as vesicles for an efficient absorption of free cholesterol.[17] It has been reported that cholesterol uptake into Caco-2 cells, an enterocyte model, from lecithin-containing micelles was accelerated by CEase.[18]

The role of CEase has been suggested to extend beyond that of hydrolyzing dietary lipids. It enhanced sterol transfer between small unilamellar phospholipid vesicles in vitro[19] and effected plasma lipoprotein metabolism.[16] Several lines of evidence indicated a role of vascular CEase in atherosclerosis. CEase may be pro-atherogenic since it facilitated the conversion of the larger and less atherogenic low-density lipoprotein particles to smaller and more atherogenic lipoprotein subspecies.[16,20] The catalytic activity of CEase led to a high degree of unesterified cholesterol within the core of low-density lipoproteins. Such modified lipoprotein species resembled aortic unilamellar and multilamellar lipid particles that accumulate in the extracellular spaces of atherosclerotic lesions.[21−23] CEase was also shown to act synergistically with sphingomyelinase to promote cholesterol crystal nucleation and aggregation

* To whom correspondence should be addressed (phone: +49 228 732317; fax: +49 228 732567; e-mail: guetschow@uni-bonn.de).

10.1021/jm0508639 CCC: $30.25
Published on Web 11/12/2005

of low-density lipoproteins. Both events are regarded to be important in atherosclerosis.[24] In contrast, CEase may be antiatherogenic by facilitating the selective uptake of high-density lipoprotein-associated cholesterol esters by liver cells and thus reducing cholesterol accumulation in peripheral tissues. Furthermore, the enzyme might reduce the atherogenicity of oxidized low-density lipoproteins by decreasing its lysophosphatidylcholine and ceramide content.[16,25−28]

Much attention has focused on the inhibition of CEase as a potential target particularly for the development of hypocholesterolemic agents. Several classes of mechanism-based inhibitors have been described including boronic and borinic acids, aryl haloketones, aryl phosphates and phosphonates as well as aryl and cholesteryl carbamates with the carbamates being the most intensive studied inhibitors of CEase.[29−32] Substituted 6-chloro-2-pyrones are representatives of a further class of potent CEase inhibitors.[33,34] 6-Chloro-3-(1-ethyl-2-cyclohexyl)-2*H*-pyran-2-one was found to inhibit the hydrolysis of cholesteryl oleate in vivo, thereby limiting the bioavailability of cholesterol derived from cholesterol esters. As a result, the appearance of cholesterol in serum and liver of hamsters was reduced in a dose-dependent manner.[17]

In a previous paper, we investigated the inhibition kinetics of the reaction of some fused 1,3-oxazin-4-ones and 1,3-thiazin-4-ones with bovine pancreatic CEase.[35] Certain thieno[1,3]oxazin-4-ones acted as alternate substrate inhibitors being hydrolyzed by CEase under steady-state conditions via an acylation−deacylation mechanism, similar to the interaction of 3,1-benzoxazin-4-ones and analogous thieno[1,3]oxazin-4-ones with serine proteases.[36−41] 2-Diethylamino-6,7-dihydro-4*H*,5*H*-cyclopenta[4,5]thieno[2,3-*d*][1,3]oxazin-4-one was shown to significantly inhibit the CEase-catalyzed cleavage of cholesterol esters in isolated human high-density lipoproteins. In that study, matrix-assisted laser desorption and ionization time-of-flight mass spectrometry (MALDI-TOF MS) was used to investigate the extracts of human lipoproteins after treatment with CEase and to monitor the effects of the inhibitor.[42]

AChE is a serine hydrolase[43] that exhibits a broad substrate specificity for various amides and esters including acyl homologues and *N*-demethylated analogues of acetylcholine. Specificity of AChE is highest for acetylselenocholine, acetylthiocholine (ATCh), and acetylcholine;[44] it hydrolyzes acetylcholine faster than other choline esters and presents little activity on butyrylcholine.[45]

The physiological role of AChE, the hydrolytic destruction of the neurotransmitter acetylcholine at cholinergic synapses, is necessary for the temporal control of cholinergic transmission. Besides this 'classical' function, AChE was reported to exhibit several 'nonclassical' activities.[45,46] The enzyme was suggested to act as an adhesion protein in synaptic development and maintenance[46] as well as to be involved in neurite growth,[47] hematopoiesis and osteogenesis.[48] In addition to these physiological functions, AChE has been shown to accelerate the pathophysiological assembly of the amyloid-β (Aβ) peptide into amyloid fibrils in vitro[49,50] and in vivo,[51,52] with complexes of AChE and Aβ displaying an enhanced neurotoxicity in comparison to fibrils formed by Aβ alone.[53,54] AChE was found to be associated with amyloid plaques and neurofibrillary tangles in Alzheimer's disease (AD) and may contribute to their development.[55−57]

AD is a slowly progressive dementia paralleled by selective neuronal cell death, which is probably caused by Aβ fibrils or oligomers.[58,59] In addition, the 'cholinergic hypothesis' was focused on the loss of cholinergic neurotransmission in AD.[60] This has provided the rationale for the current major therapeutic approach to AD, the inhibition of the catalytic function of AChE, thereby increasing the bioavailability of acetylcholine at the synaptic cleft and improving the cholinergic neurotransmission as well as the cognitive functions.[61,62] Tacrine (Cognex), donepezil (Aricept), galanthamine (Reminyl) and rivastigmine (Exelon) are currently approved AChE inhibitors for the treatment of AD.[63] Beside its central role in the therapy of AD, AChE has been targeted in treatments for myasthenia gravis, glaucoma, obstipation, and spasmolysis and to antagonize muscle relaxation in anesthesiology.[64]

While the catalytic function is associated to the active site of AChE, the peripheral anionic site (PAS) modulates the 'nonclassical' activities of the enzyme.[65] The PAS was shown to be involved in an accelerated Aβ fibril formation, and thus, low molecular weight compounds that bind to PAS as well as a PAS-directed monoclonal antibody did not only inhibit the catalytic activity but also prevented the amyloidogenic effect of AChE.[66,67] On the other hand, AChE inhibitors that primarily interact with the active site had no effect on amyloid polymerization.[63] The PAS, situated at the surface of AChE, is connected with the active site by a deep and narrow gorge (around 20 Å long), lined by fourteen highly conserved aromatic residues. The active site is located at the bottom of the gorge and consists of the esteratic site, where hydrolysis proceeds via the catalytic triad Ser200-His440-Glu327 (*Torpedo californica* AChE numbering),[68] as well as the anionic site with the indole ring of the conserved Trp84, that has been shown to interact with the quaternary ammonium group of acetylcholine via a cation−π interaction.[46,68] Another conserved aromatic residue, Phe330, is also involved in this interaction. Similarly, the principal element of PAS is the indole of Trp279.[69]

Considering the role of the PAS relative to its involvement in the processes of AD, the development of dual site inhibitors of AChE, e.g. acyloxybiphenyl carbamates,[70] donepezil and AP2238,[71] is driven by the fact that they may simultaneously alleviate the cognitive deficit in AD due to inhibition of the catalytic activity and avoid the assembly of Aβ by interacting with the PAS.

On the basis of these considerations and previous results,[35] we have prepared a series of thieno[1,3]oxazin-4-ones and thieno[1,3]thiazin-4-ones and investigated their ability to inhibit bovine pancreatic CEase as well as AChE from *Electrophorus electricus*. The interaction of selected compounds with the target esterases was kinetically characterized. As it is demonstrated in the results section, two concepts, the alternate substrate inhibition of CEase and a dual site inhibition of AChE, have been implemented in this study.

Scheme 1[a]

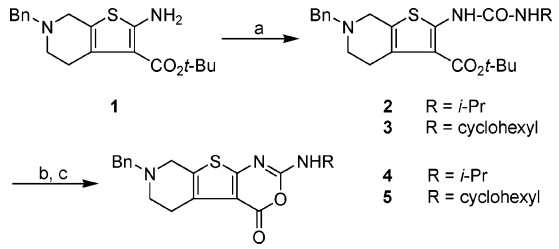

[a] Reagents: (a) RNCO, pyridine, 70 °C; (b) TFA, trifluoroacetic anhydride, 0−25 °C; (c) H_2O, $NaHCO_3$, 0 °C.

Scheme 2[a]

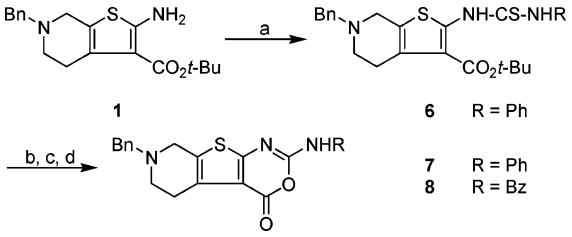

[a] Reagents: (a) phenyl isothiocyanate, C_2H_5OH, 80 °C (**6**, R = Ph), or benzoyl isothiocyanate, CH_3COCH_3, room temperature (**6**, R = Bz was used in the next step without purification); (b) TFA, 0−25 °C; (c) H_2O, $NaHCO_3$, 0 °C; (d) HgO, CH_2Cl_2, room temperature.

Scheme 3[a]

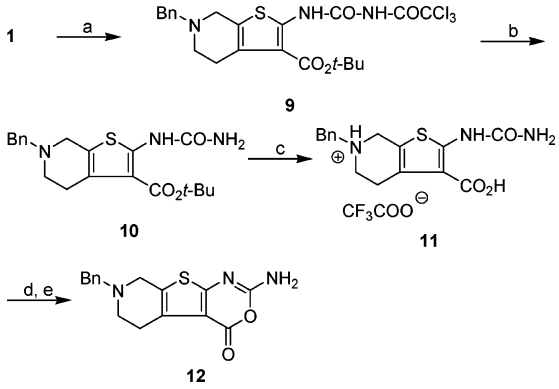

[a] Reagents: (a) trichloroacetyl isocyanate, THF, 0−10 °C; (b) CH_3OH, THF, 60 °C; (c) TFA, 0−25 °C; (d) trifluoroacetic anhydride, TFA, 0−25 °C; (e) CH_3OH/H_2O, $NaHCO_3$, 0 °C.

Results and Discussion

Synthesis. The Gewald thiophene synthesis[72,73] allowed for a facile synthetic entry to the classes of thieno[2,3-*d*][1,3]oxazin-4-ones and thieno[2,3-*d*][1,3]thiazin-4-ones. Tertiary butyl ester (Schemes 1−5) or ethyl ester (Scheme 6) of 2-aminothiophene-3-carboxylates were used as starting materials to prepare the final thieno[2,3-*d*][1,3]oxazin-4-ones and thieno[2,3-*d*][1,3]thiazin-4-ones, respectively. The requisite aminothiophenes **1** and **26**−**32** (Scheme 5) were synthesized from the appropriate ketone, sulfur, and *tert*-butyl cyanoacetate in the presence of morpholine by an one-pot thiolation−heterocyclization reaction. To afford **25** (Scheme 5), the Knoevenagel adduct of cyclopentanone and *tert*-butyl cyanoacetate was prepared and subsequently treated with sulfur in the presence of diethylamine.

2-Alkylamino-substituted thienoxazinones (Scheme 1) were synthesized according to the procedure of Hallenbach et al.[74] Aminothiophene **1** was reacted with isopropyl isocyanate or cyclohexyl isocyanate in pyridine to yield ureas **2** and **3**, respectively. Subsequent treatment with a mixture of trifluoroacetic acid and trifluoroacetic anhydride resulted in deesterification and cyclocondenstaion, to obtain **4** and **5**.

The preparation of 2-phenylamino- and 2-benzoylamino-substituted thienoxazinones is shown in Scheme

Scheme 4[a]

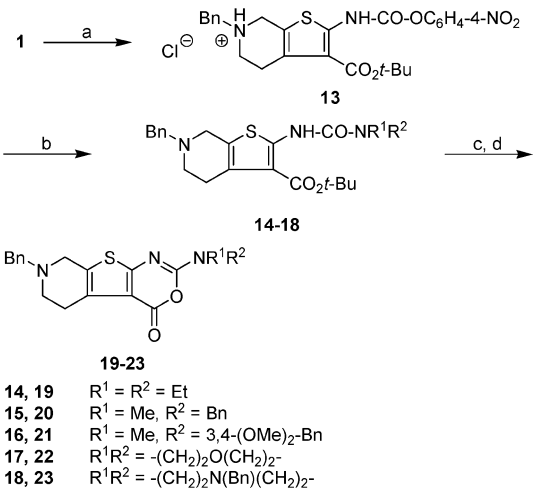

14, 19	$R^1 = R^2$ = Et
15, 20	R^1 = Me, R^2 = Bn
16, 21	R^1 = Me, R^2 = 3,4-$(OMe)_2$-Bn
17, 22	R^1R^2 = -$(CH_2)_2O(CH_2)_2$-
18, 23	R^1R^2 = -$(CH_2)_2N$(Bn)$(CH_2)_2$-

[a] Reagents: (a) *p*-nitrophenyl chloroformate, pyridine, $Cl(CH_2)_2Cl$, 0 °C; (b) HNR^1R^2, $Cl(CH_2)_2Cl$, 0 °C (**14**, **18**), or 0−25 °C (**15**−**17**); (c) TFA, trifluoroacetic anhydride, 0−25 °C (**19**, **20**, **22**, **23**), or TFA, 0 °C, then trifluoroacetic anhydride, CH_2Cl_2, 0−4 °C (**21**); (d) H_2O, $NaHCO_3$, 0 °C (**19**, **20**, **22**, **23**), or CH_3OH/H_2O, $NaHCO_3$, 0 °C (**21**).

Scheme 5[a]

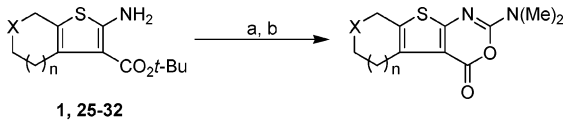

25, **33**	n = 0, X = CH_2
26, **34**	n = 1, X = CH_2
27, **35**	n = 1, X = O
28, **36**	n = 1, X = S
29, **37**	n = 1, X = N-Me
30, **38**	n = 1, X = N-Et
31, **39**	n = 1, X = N-*i*-Bu
1, **40**	n = 1, X = N-Bn
32, **41**	n = 1, X = N-Bz

[a] Reagents: (a) dichloromethylene dimethylammonium chloride, 1 M ethereal HCl, $Cl(CH_2)_2Cl$, reflux; (b) *n*-hexane, reflux (**33**, **35**, and **36**), or C_2H_5OH/H_2O, 0 °C (**34**), or H_2O, Na_2CO_3, 0 °C (**37**−**40**).

Scheme 6[a]

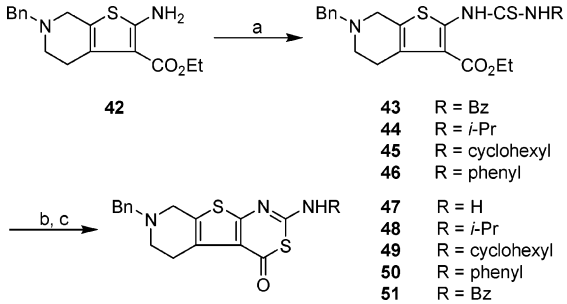

[a] Reagents: (a) benzoyl isothiocyanate, CH_3COCH_3 (**43**) or RNCS, C_2H_5OH (**44**−**46**), reflux; (b) 94% H_2SO_4, room temperature − 100 °C (**47** from **43**), or concd H_2SO_4, room temperature (**48**−**50**, **51** from **43**); (c) H_2O, NaOH, 0 °C (**47**, **49**−**51**), or H_2O, $NaHCO_3$, 0 °C (**48**).

2. The thiourea derivative **6** was easily obtained from aminothiophene **1** and phenyl isothiocyanate. Deprotection of **6** with trifluoroacetic acid followed by cyclization using yellow mercury(II) oxide in dichloromethane[39] at room temperature furnished the final product **7**. Compound **8** was similarly prepared without isolating the thiourea intermediate.

The synthetic route to the 2-aminothienoxazin-4-one **12** is outlined in Scheme 3. Aminothiophene **1** was converted to urea **9** by the action of trichloroacetyl isocyanate. Cleavage of the trichloroacetyl residue with methanol yielded **10**, which was reacted with trifluoroacetic acid to obtain the 2-ureidothiophene-3-carboxylic acid **11**. Ring closure to **12** was then performed upon the action of trifluoroacetic anhydride.

The synthesis of 2-secondary-amino-substituted thienoxazinones **19**−**23** was accomplished by a novel route shown in Scheme 4. The urethane hydrochloride **13** was easily obtained by the reaction of the aminothiophene **1** with *p*-nitrophenyl chloroformate in the presence of pyridine. Nucleophilic attack of secondary amines at the activated urethane carbonyl readily afforded ureas **14**−**18**, which were subsequently cyclized to the desired thienoxazinones.

2-Dimethylamino-substituted thienoxazinones **33**−**41** (Scheme 5) were synthesized by a facile one-step route according to Player et al.[75] Aminothiophenes **1** and **25**−**32** were reacted with dichloromethylene dimethylammonium chloride in the presence of ethereal hydrochloric acid to form the hydrochlorides of the desired products. Treatment of the hydrochlorides with boiling *n*-hexane (**33**, **35**, and **36**) or 50% C_2H_5OH (**34**), purification by column chromatography (**41**), or addition of a saturated sodium carbonate solution followed by column chromatography (**37**−**40**) yielded the thienoxazinones **33**−**41**.

The preparation of thienothiazin-4-ones is shown in Scheme 6. In contrast to the synthetic routes to afford the thienoxazinones via *tert*-butyl precursors (Schemes 1-5), the thienothiazinones **47**−**51** were prepared by a route using the ethyl 2-aminothiophenecarboxylate **42** as starting material. Treatment with isothiocyanates gave the thiourea derivatives **43**−**46**. Ring closure to **47**−**51** was then performed upon the action of concentrated sulfuric acid, according to previously reported procedures.[76,77]

Alkaline Hydrolysis. Stability of the compounds was measured spectrophotometrically in aqueous buffer, pH 11.0, at 25 °C. Alkaline hydrolysis rate constants of the thieno[1,3]oxazin-4-ones as well as the thieno[1,3]-thiazin-4-ones were determined by the disappearance of the long-wavelength ultraviolet chromophore that followed the first-order exponential decay. The decade logarithms of the second-order rate constant, log k_{OH^-}, were calculated and outlined in Tables 1−4. In comparison to thienoxazinones with a disubstituted 2-amino group, compounds **4**, **5**, and **7** bearing a monosubstituted 2-amino moiety showed an increased stability (log $k_{OH^-} \leq -1.90$) which might arise from deprotonation at the 2-amino substituent.[78,79] Resonance stabilization of the negative charge in thieno[1,3]oxazin-4-ones reduces the electrophilicity at C-4 carbon. As described,[38,39] aqueous alkaline hydrolysis proceeds by hydroxide attack at C-4 to produce the corresponding ureidothiophenecarboxylic acids and thieno[2,3-*d*]pyrimidin-2,4-diones, respectively. Benzoylamino derivatives **8** and **51** (Table 4) are the most acidic substances of the present series, and hence, no conversion was observed at pH 11 over a period of 24 h. Both the alkaline hydrolysis of thieno-[1,3]oxazin-4-ones and the process by which they inhibit CEase involve an attack of a nucleophilic oxygen upon the C-4 carbonyl carbon. Structural features promoting enzyme inhibition over chemical reactivity are crucial for the design of heterocyclic alternate substrate inhibitors.

Inhibition of CEase and AChE. The kinetic parameters of the inhibition of CEase and AChE by 36 compounds were determined spectrophotometrically and are given in Tables 1−4. CEase inhibition was assayed in the presence of *p*-nitrophenyl butyrate (pNPB) as a chromogenic substrate. K_i values toward CEase were obtained from measurements in the presence of a single concentration or at various concentrations of the inhibitor, [I], in consideration of the substrate concentration and a formal competitive type of inhibition.

The activity of AChE was determined in a coupled assay with the substrate ATCh and 5,5′-dithio-bis-(2-nitrobenzoic acid) (DTNB). Active inhibitors of AChE were used at five or six different concentrations. Plots of the rates versus [I], however, did not become asymptotic to the *x*-axis. A residual activity at infinite concentration of the inhibitor, $v_{[I]\to\infty}$, had to be considered. The value of $v_{[I]\to\infty}$ at a defined substrate concentration can be obtained from a plot of the rates versus [I] and nonlinear regression according to eq 1,

$$v = \frac{(v_0 - v_{[I]\to\infty})}{\left(1 + \frac{[I]}{IC_{50}}\right)} + v_{[I]\to\infty} \qquad (1)$$

where v_0 is the velocity in the absence of the inhibitor. The IC_{50} value calculated by this equation corresponds to the concentration of the inhibitor which reduces the rate of the enzyme-catalyzed reaction to a velocity $(v_0 - v_{[I]\to\infty})/2 + v_{[I]\to\infty}$, i.e. the velocity half between v_0 and $v_{[I]\to\infty}$. Data $v_{[I]\to\infty}$ as relative velocities with respect to v_0, as well as IC_{50} values are given in Tables 1−4. To judge the potency of inhibitors of AChE mainly IC_{50} but also the values $v_{[I]\to\infty}$ were taken into account.

Inhibition of the target enzymes by 2-diethylamino-substituted oxazinones is shown in Table 1. Different residues R^5 and R^6 were introduced or formed together with two thiophene carbons a further fused ring. Polar groups, such as $CONH_2$ in compound **55** or the basic tetrahydropyridine unit in **19**, were unfavorable for an inhibition of CEase. In contrast, nonpolar moieties, particularly when forming a bridged ring system, resulted in potent inhibition of CEase. K_i values less than 2 μM were determined for compounds with cycloaliphatic five- and six-membered rings. The methyl-branched derivative **58** was found to be similarly active as **56** and **57**, which have already been described in a previous study.[35] When the 5-isopropyl residue in **53** was connected with the thiophene C-6 carbon by an ethylene bridge, the enhanced rigidity promoted a 4-fold increase in potency (**53** versus **58**). However, ring closure of **54** with a methylene unit also resulted in pronounced inhibition (**54** versus **56**), an effect that can rather be

Table 1. Inhibition of Bovine CEase and AChE from *Electrophorus electricus*[a]

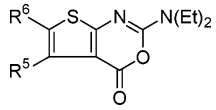

compd	R^5	R^6	CEase K_i (μM)	AChE IC_{50} (μM)	AChE $v_{[I]\to\infty}$[b]	log k_{OH^-} (M^{-1} s^{-1})
52	Me	H	15	>50	–	−1.14[c]
53	*i*-Pr	H	6.4	>50	–	−1.27[c]
54	Me	Me	4.3	>50	–	−1.63[c]
55	Me	$CONH_2$	>50	>50	–	−0.40[d]
56	-$(CH_2)_3$-		0.58 ± 0.05[e]	>50	–	−1.03[c]
57	-$(CH_2)_4$-		1.86 ± 0.05[e]	>50	–	−1.59[d]
58	-CH(Me)$(CH_2)_3$-		1.64 ± 0.05	>50	–	−1.41[c]
59	-$(CH_2)_5$-		6.0	>50	–	−1.42[c]
60	-CH=CH−CH=CH-		7.5	>50	–	−1.13[c]
19	-$CH_2CH_2N(Bn)CH_2$-		>50	2.08 ± 0.07	0.061 ± 0.004	−1.35

[a] Values with standard error were calculated from duplicate experiments at five or six inhibitor concentrations; those without standard error are mean values of duplicate inhibition experiments at a single inhibitor concentration. [b] Values of $v_{[I]\to\infty}$ were calculated relative to v_0. [c] Data from ref 39. [d] Data from ref 38. [e] Data from ref 35.

Table 2. Inhibition of Bovine CEase and AChE from *Electrophorus electricus*[a]

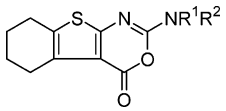

compd	R^1	R^2	CEase K_i (μM)	AChE IC_{50} (μM)	AChE $v_{[I]\to\infty}$	log k_{OH^-} (M^{-1} s^{-1})
61	H	*i*-Pr	>50	>50	–	−0.49[b]
34	Me	Me	2.15 ± 0.19	>50	–	−1.24
57[c]	Et	Et	1.86 ± 0.05[d]	>50	–	−1.59[b]
62	Me	cyclohexyl	18	>50	–	−0.79
63	-$(CH_2)_2O(CH_2)_2$-		5.7	>50	–	−1.08[b]

[a] Values with standard error were calculated from duplicate experiments at five or six inhibitor concentrations; those without standard error are mean values of duplicate inhibition experiments at a single inhibitor concentration. [b] Data from ref 38. [c] Data are also noted in Table 1. [d] Data from ref 35.

attributed to an enhancement in lipophilicity than in rigidity. A further variation in the size of the fused cycloaliphatic moiety diminished activity as in case of **59** bearing a seven-membered ring.

Among the compounds outlined in Table 1, inhibition of AChE was determined only for the tetrahydropyrido derivative **19**. Compound **19** is different from the other 2-diethylamino derivatives in Table 1 in that it bears a bulky benzyl residue attached at a basic nitrogen. This finding prompted us to design a series of analogues of the parent **19** to further elucidate structure−activity relationships of tetrahydropyrido-anellated thieno[1,3]-oxazinones as inhibitors of AChE. The corresponding results are presented below (Table 3, Table 4).

The tetramethylene bridge of **57** was then maintained and different amino groups were introduced at position 2 (Table 2). Dimethylamino substitution in **34** provided an additional potent inhibitor of CEase. The increased steric requirement of the cyclohexyl methylamino group was unfavorable (**62** versus **34**) as well as the polar connection of the ethyl rests of **57** as achieved in the morpholino derivative **63**. As expected from the aforementioned results, such tetramethylene compounds did not inhibit AChE.

Our next approach was to attain structural diversity in the ring fused to the thiophene nucleus of thieno-[1,3]oxazinones (Table 3). The 2-dimethylamino moiety, as it occurs in **34**, was retained unchanged. In accordance to the data from the 2-diethylamino series, ring

Table 3. Inhibition of Bovine CEase and AChE from *Electrophorus electricus*[a]

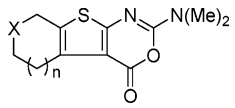

compd	*n*	X	CEase K_i (μM)	AChE IC_{50} (μM)	AChE $v_{[I]\to\infty}$[b]	log k_{OH^-} (M^{-1} s^{-1})
33	0	CH_2	0.63 ± 0.03	>50	–	−1.13
34[c]	1	CH_2	2.15 ± 0.19	>50	–	−1.24
35	1	O	>50	>50	–	−1.00
36	1	S	5.76 ± 0.23	>50	–	−1.05
37	1	N-Me	>50	38.9 ± 1.2	0.076 ± 0.006	−0.98
38	1	N-Et	>50	10.5 ± 0.5	0.064 ± 0.006	−0.99
39	1	N-*i*-Bu	>50	0.36 ± 0.01	0.043 ± 0.002	−1.16
40	1	N−Bn	>50	0.89 ± 0.02	0.066 ± 0.003	−0.97
41	1	N−Bz	>50	35.6 ± 1.7	0.266 ± 0.010	−0.79

[a] Values with standard error were calculated from duplicate experiments at five or six inhibitor concentrations; those without standard error are mean values of duplicate inhibition experiments at a single inhibitor concentration. [b] Values of $v_{[I]\to\infty}$ were calculated relative to v_0. [c] Data are also noted in Table 2.

contraction to the fused cyclopentene-containing analogue increased CEase inhibition. The resulting inhibitor **33** exhibited a K_i value of 630 nM. The 7-methylene group of **34** was exchanged for sulfur or oxygen. The increasing polarity of the carbon−sulfur and carbon−oxygen bonds was still tolerated in the former case **36** but gave an inactive tetrahydropyran derivate **35**. Basic tetrahydropyridines **37**−**40** confirmed this tendency.

Table 4. Inhibition of Bovine CEase and AChE from *Electrophorus electricus*[a]

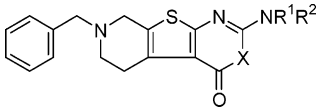

				CEase	AChE		
compd	R^1	R^2	X	K_i (μM)	IC_{50} (μM)	$v_{[I]\to\infty}$[b]	log k_{OH^-} (M^{-1} s^{-1})
12	H	H	O	>50	5.90 ± 0.20	0.056 ± 0.006	−1.47
47	H	H	S	>50	1.20 ± 0.05	0.045 ± 0.004	−2.25
4	H	*i*-Pr	O	>50	0.74 ± 0.44	0.544 ± 0.035	−1.97
48	H	*i*-Pr	S	>50	0.58 ± 0.03	0.137 ± 0.006	−2.18
5	H	cyclohexyl	O	>50	–	0.806 ± 0.008	−2.42
49	H	cyclohexyl	S	>50	2.82 ± 0.22	0	−2.15
7	H	Ph	O	>50	0.94 ± 0.24	0.550 ± 0.018	−1.90
50	H	Ph	S	>50	1.03 ± 0.07	0.213 ± 0.012	−1.70
8	H	Bz	O	>50	2.86 ± 0.21	0.064 ± 0.012	–[c]
51	H	Bz	S	>50	5.2	–	–[c]
40[d]	Me	Me	O	>50	0.89 ± 0.02	0.066 ± 0.003	−0.97
19[e]	Et	Et	O	>50	2.08 ± 0.07	0.061 ± 0.004	−1.35
20	Me	Bn	O	>50	0.84 ± 0.07	0.212 ± 0.008	−0.51
21	Me	3,4-$(OMe)_2$−Bn	O	>50	0.33 ± 0.01	0.042 ± 0.004	−1.24
22	-$(CH_2)_2O(CH_2)_2$-		O	>50	0.77 ± 0.07	0.059 ± 0.011	−0.82
23	-$(CH_2)_2N(Bn)(CH_2)_2$-		O	>50	1.32 ± 0.13	0.085 ± 0.014	−1.06

[a] Values with standard error were calculated from duplicate experiments at five or six inhibitor concentrations; those without standard error are mean values of duplicate inhibition experiments at a single inhibitor concentration. [b] Values of $v_{[I]\to\infty}$ were calculated relative to v_0. [c] No conversion was observed after 24 h. [d] Data are also noted in Table 3. [e] Data are also noted in Table 1.

These tertiary amines were inactive toward CEase as the nonbasic, but polar benzamide **41**. The following structure−activity relationships could be deduced from the data shown in Tables 1−3, (i) a dimethylamino or diethylamino group at position 2 and (ii) a cycloaliphatic five- or six-membered ring fused at the thiophene were favorable for CEase inhibition. Accordingly, 14 other derivatives that did not fulfill these requirements were inactive (Table 4).

From the data in Table 3, significant structure−activity relationships could also be ascertained for AChE inhibition. A nitrogen at position 7 was necessary to obtain anticholinesterases (**33**-**36** versus **37**-**41**), but not sufficient for strong inhibition which required a lipophilic substituent at a basic nitrogen. The isobutyl and the benzyl compound (**39** and **40**) showed IC_{50} values toward AChE in the nanomolar range. Noteworthy, the extension of the methyl rest in **37** by an isopropyl or a phenyl group in **39** or **40**, respectively, increased inhibitory potency by 2 orders of magnitude.

N-Benzyl substitution at the tetrahydropyrido unit of tricyclic thieno[1,3]oxazinones was found to be advantageous for AChE inhibition (**19**, Table 1; **40**, Table 3). This substructure was therefore maintained whereas the 2-amino substituent was varied and the ring oxygen was replaced by sulfur in certain cases (Table 4). In general, the representatives of the so defined structure exhibited AChE inhibiting potency. The differences between the NH_2-, primary-amino and secondary-amino derivatives were rather small. The exchange of the ring oxygen for sulfur did not substantially alter the IC_{50} values. The residual activity at infinite inhibitor concentration ($v_{[I]\to\infty}$) was found to be lowered in case of the thieno[1,3]thiazin-4-ones (**12**, **4**, **5**, **7**, X = O, versus **47**-**50**, X = S). When one methyl group of the dimethylamino compound **40** was replaced by benzyl, the same IC_{50} value but an increased residual activity was determined (**40** versus **20**). However, exchange of one methyl group in **40** for 3,4-dimethoxybenzyl led to the most active AChE inhibitor of the present series (**40** versus **21**). Compound **21** had an IC_{50} value of 330 nM and showed the lowest residual activity of all compounds investigated.

Kinetic Characterization of the Inhibition of CEase. In a previous study we have demonstrated that thieno[1,3]oxazin-4-ones have the capability to act as alternate substrate inhibitors of CEase, provided that the enzyme-catalyzed consumption of the inhibitor occurs under steady-state conditions. Due to the accumulation of an enzyme−inhibitor complex, the transformation followed a zero-order kinetics. An essential conclusion that was derived from the general kinetic model is the concurrence of the K_i value of a given inhibitor and the separately determined Michaelis constant, K_m^I, of its enzymatic consumption.[35]

The kinetic characterization of the new CEase inhibitor **33** was done as follows. Five different concentrations of **33** were used, and the rates were plotted against the inhibitor concentrations (Figure 1). A value K_i $(1 + [S]/K_m^S) = 1.78$ μM was obtained, and a value $K_i = 0.63$ μM (Table 3) could be calculated from the respective substrate concentration, [S], and a value of 110 μM for the Michaelis−Menten constant, K_m^S, of the chromogenic substrate pNPB. To reveal the type of inhibition, reactions were measured in the presence of different substrate concentrations and the data were analyzed according to the Hanes−Woolf method (Figure 2). The [S]/v versus [S] plot (Figure 2a) showed parallel lines indicating a formal competitive type of inhibition. The secondary plot of the intercepts versus [I] and a linear regression gave $K_i = 0.68$ μM (Figure 2b). This value was in accordance with the calculated one (Table 3), and thus the competitive mode was confirmed and the inhibitor could be characterized as active site-directed.

Next, the enzyme-catalyzed consumption of **33** was examined and a general kinetic model for alternate substrate inhibition via acyl enzymes was used.[35] The enzymatic turnover of compound **33** at an initial con-

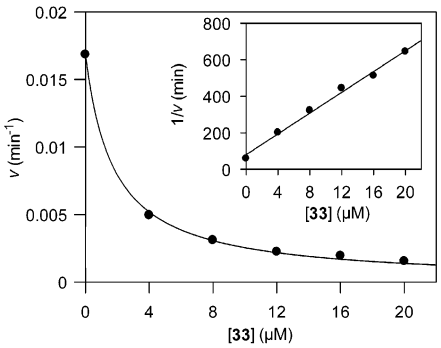

Figure 1. Inhibition of CEase by compound **33.** Plot of the rates versus [I] for the inhibition of CEase by compound **33** in 100 mM sodium phosphate, 100 mM NaCl, pH 7.0 with 6 mM TC, 6% acetonitrile and 10 ng/mL CEase. Initial substrate concentration was 200 μM pNPB. Rates were obtained by linear regression of the progress curves (not shown) and are mean values of duplicate experiments. The solid line was drawn using the best-fit parameters from a fit according to an equation of competitive inhibition, which gave K_i $(1 + [S]/K_m^S) = 1.78 \pm 0.08$ μM. The insert is a Dixon plot to show the linearity.

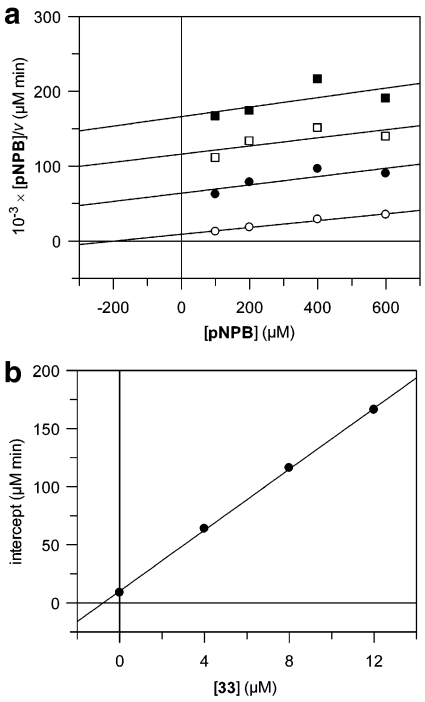

Figure 2. Inhibition of CEase by compound **33** in the presence of different concentrations of the chromogenic substrate pNPB. (a) Hanes−Woolf plot using mean values of rates from duplicate experiments in 100 mM sodium phosphate, 100 mM NaCl, pH 7.0 with 6 mM TC, 6% acetonitrile and 10 ng/mL CEase. Concentrations of compound **33** were as follows: open circles, [I] = 0; full circles, [I] = 4 μM; open squares, [I] = 8 μM; full squares, [I] = 12 μM. Linear regression gave values for vertical intercepts. (b) Plot of vertical intercepts versus the concentrations of compound **33**. Linear regression according to equation, intercept $= [K_m^S\,[I]/(K_i\,V_{max}^S)] + (K_m^S/V_{max}^S)$, gave a slope $K_m^S/(K_i\,V_{max}^S) = 13.1 \pm 0.2$ min, that corresponds to a value $K_i = 0.68 \pm 0.01$ μM.

centration of 25 μM was investigated in the presence of a high CEase concentration (~730-fold higher compared with the inhibition experiments in the presence of pNPB). Spectral changes were monitored in 10 min intervals (Figure 3a). The final spectra revealed the corresponding 2-(3,3-dimethylureido)thiophene-3-carboxylic acid as the product. Its formation can easily be explained by a nucleophilic attack of the active site serine at the C4-carbon of **33** to give an intermediate acyl-enzyme which subsequently undergoes hydrolytic cleavage. A similar conversion of the thieno[1,3]oxazin-4-one **56** to the corresponding 2-(3,3-diethylureido)-thiophene-3-carboxylic acid has been shown previously.[35] The time-dependent decrease of the concentration of **33** monitored at a fixed wavelength is depicted in Figure 3b. The reaction followed zero-order kinetics until the hydrolysis was nearly finished. These data were used for a plot (Figure 3c) according to an integrated form of the Michaelis−Menten equation.

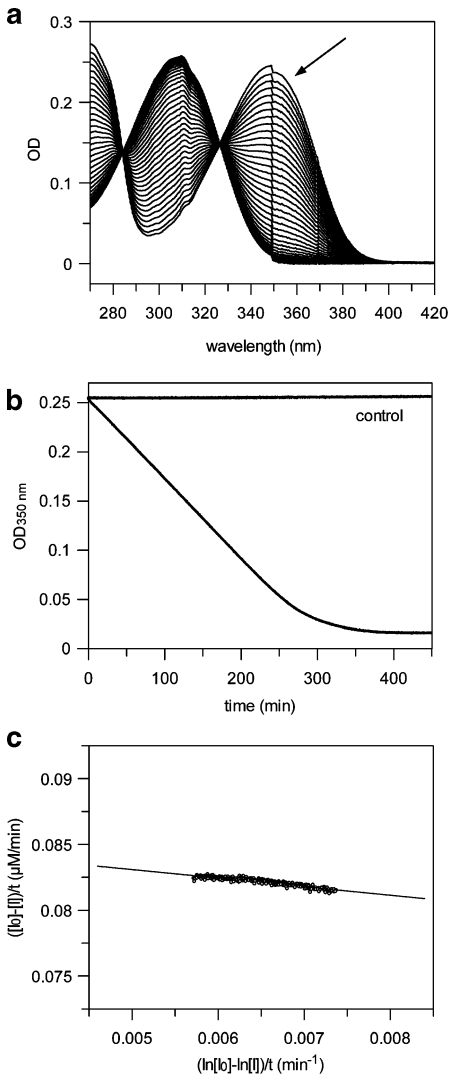

Figure 3. Kinetics of the CEase-catalyzed hydrolysis of compound **33**. Reaction was performed in 100 mM sodium phosphate, 100 mM NaCl, pH 7.0 with 6 mM TC, 6% acetonitrile, and an adjusted activity of CEase. Initial concentration of compound **33**, $[I_0]$, was 25 μM. (a) Depletion of compound **33** is illustrated by monitoring UV/vis-spectra at 10 min-intervals. The *arrow* indicates the initial spectrum. (b) Hydrolysis of compound **33** was followed at 350 nm. Control reaction in the absence of CEase is shown to demonstrate the stability of compound **33**. (c) Plot $([I_0] - [I])/t$ versus $(\ln[I_0] - \ln[I])/t$, where $[I_0]$ is the initial concentration of the inhibitor **33** and [I] is the inhibitor concentration at the time t. The values for [I] at $t = 200-250$ min based on the data shown in part b. Linear regression gave a negative slope of 0.65 ± 0.02 μM that corresponds to K_m^I and an intercept of $V_{max}^I = 0.086 \pm 0.001$ μM min^{-1}.

Table 5. Kinetic Parameters of the CEase-Catalyzed Turnover of Thieno[1,3]oxazin-4-ones

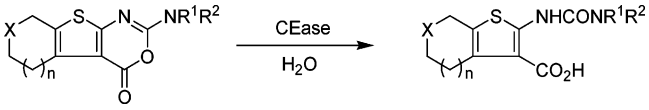

compd	*n*	X	R^1	R^2	K_m^I (μM)	V_{max}^I (μM min^{-1})	V_{max}^I/K_m^I (min^{-1})
33[a]	0	CH_2	Me	Me	0.65 ± 0.02	0.086 ± 0.001	0.13
56[b]	0	CH_2	Et	Et	0.65 ± 0.05	0.533 ± 0.003	0.82
35	1	O	Me	Me	>25	>0.033[c]	0.0013
40	1	N−Bn	Me	Me	>25	>0.030[c]	0.0012

[a] An molar extinction coefficient $\epsilon = 9.84$ mM^{-1} cm^{-1} was used to determine K_m^I and V_{max}^I. [b] $\epsilon = 9.97$ mM^{-1} cm^{-1}. [c] The limits were defined according to $V_{max}^I > [I_0]\ V_{max}^I/K_m^I$.

Values for maximum velocity, V_{max}^I, and for the Michaelis constant, K_m^I, of the enzymatic consumption of the inhibitor could be obtained, and V_{max}^I/K_m^I could therewith be calculated (Table 5). The enzyme-catalyzed conversion was similarly inspected for compounds **35** and **40** (Table 5) with an equal CEase activity adjusted toward pNPB prior to the experiments. Compound **56** was reinvestigated[35] in order to obtain a V_{max}^I value that could be compared with those of the other compounds.

Thieno[1,3]oxazinones **33** and **56** could be classified as true alternate substrate inhibitors of CEase based on the concurrence of the K_i and K_m^I values. Compound **33** had a K_i of 0.63 μM (Table 3) and a K_m^I of 0.65 μM (Table 5), **56** exhibited a K_i of 0.58 μM (Table 1) and a K_m^I of 0.65 μM (Table 5). Although both compounds are equally potent as inhibitors of CEase, the new thieno-[1,3]oxazinone **33** is superior in terms of resistance to enzymatic degradation. The relevant parameter is V_{max}^I being 6-fold lower in the case of **33**. It can be concluded that the acyl-enzyme, E−I, derived from the reaction of CEase with **33** undergoes an accordingly decelerated hydrolytic deacylation. The alternate substrate mode of CEase inhibition by **33** and **56** can analogously be supposed for the other active compounds of the present series (K_i < 20 μM; Tables 1−3).

When incubating the tetrahydropyrano derivative **35** and the tetrahydropyrido derivative **40**, respectively, with the same amount of CEase, a very slow consumption was observed. The reaction was monitored over 66 h and followed a first-order kinetics over the entire time course. The first-order rate constants that correspond to V_{max}^I/K_m^I were obtained by nonlinear regression (Table 5). Compounds **35** and **40** are very poor substrates of CEase. Their V_{max}^I/K_m^I values are 2 orders of magnitude lower than that of **33**. To evaluate compound **35** and **40** as alternate substrate inhibitors, the reaction order of the enzymatic turnover is meaningful. Even at the initial concentration of 25 μM, the first-order kinetics indicated that an accumulation of an enzyme−inhibitor complex did not occur. Likewise it can be reasoned that compounds **35** and **40** have a K_m^I value higher than 25 μM. Their affinity to bind to CEase is low, and this conclusion is in accordance with their failure to affect CEase in the inhibition assay (K_i > 50 μM, Table 3).

Kinetic Characterization of the Inhibition of AChE. A kinetic model for the inhibition of acetylcholinesterase was considered that is outlined in Scheme 7. This model represents the general situation where the substrate, S, and the inhibitor, I, bind to the enzyme, E, at different sites, thus allowing for the formation of both an enzyme−inhibitor complex, EI, as well as an enzyme−substrate−inhibitor complex, ESI. The corresponding dissociation constants of ES and EI are K_S and K_i, respectively. The dissociation constants of the ternary complex, ESI, are αK_S and αK_i. Since the overall equilibrium constant for the formation of ESI must be the same regardless of a path via ES or via EI, the same factor α has to be included in the model.[80,81] The complex ESI is still functional with a decreased rate of product formation governed by the catalytic constant, βk_P. This type of inhibition was referred to as hyperbolic mixed-type inhibition, as the shape of a reciprocal velocity, $1/v$, versus [I] plot is hyperbolic,[80,82] and the factor α is finite and different from 1. In the case of linear inhibition with $\beta = 0$, the kinetic analysis using the Lineweaver−Burk plot, or the similar Hanes−Woolf plot, and corresponding secondary plots provides the parameters of enzyme inhibition. However, a more complex situation arises for hyperbolic inhibition with $\beta \neq 0$. For example, with Lineweaver−Burk analysis, the common replots are hyperbolic and a further reciprocal replot has to be done for linearization.[80] Baici has ingeniously presented the specific velocity plot to overcome these difficulties.[81] We intended to use the well-established Hanes−Woolf plot, $[S]/v$ versus [S], which is preferable to the double reciprocal Lineweaver−Burk plot, $1/v$ versus 1/[S], since the Hanes−Woolf plot exhibit less variation in accuracy.[83,84] Thus, a new alternative algorithm was derived to calculate kinetic parameters of hyperbolic mixed-type inhibition of AChE.

Scheme 7. Kinetic Model for the Interaction of Hyperbolic Mixed-Type Inhibitors with AChE

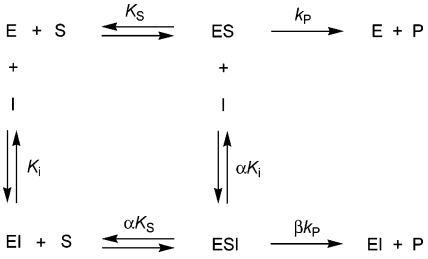

The Michaelis−Menten equation valid for the general type of inhibition as depicted in Scheme 7 is as follows.

$$v = \frac{V_{max}[S]}{\alpha K_S\left(\frac{[I] + K_i}{\beta[I] + \alpha K_i}\right) + [S]\left(\frac{[I] + \alpha K_i}{\beta[I] + \alpha K_i}\right)} \qquad (2)$$

At infinitely high inhibitor concentrations, the product is exclusively formed from ESI with a rate constant βk_P. Under this conditions, the rate, $v_{[I]\to\infty}$, at a given substrate concentration is defined by eq 3.

$$v_{[I]\to\infty} = \frac{\beta V_{max}[S]}{\alpha K_S + [S]} \qquad (3)$$

Subtractive combination of eqs 2 and 3 gave eq 4, which was simplified for the cases $\beta \neq 0$, [I] = 0 (eq 5), $\beta = 0$, [I] ≠ 0 (eq 6), and $\beta = 0$, [I] = 0 (eq 7). With $\beta = 0$, the rate $v_{[I]\to\infty}$ becomes zero. Those portion of the

product formation that results only from the decay of ES is named $v_{\beta=0}$.

$$v - v_{[I]\to\infty} = \left(\frac{(\alpha-\beta)K_S + (1-\beta)[S]}{\alpha K_S + [S]}\right)\left(\frac{V_{max}[S]}{K_S\left(1+\frac{[I]}{K_i}\right) + [S]\left(1+\frac{[I]}{\alpha K_i}\right)}\right) \quad (4)$$

$$v_0 - v_{[I]\to\infty} = \left(\frac{(\alpha-\beta)K_S + (1-\beta)[S]}{\alpha K_S + [S]}\right)\left(\frac{V_{max}[S]}{K_S + [S]}\right) \quad (5)$$

$$v_{\beta=0} = \frac{V_{max}[S]}{K_S\left(1+\frac{[I]}{K_i}\right) + [S]\left(1+\frac{[I]}{\alpha K_i}\right)} \quad (6)$$

$$v_0 = \frac{V_{max}[S]}{K_S + [S]} \quad (7)$$

Equation 8 is another expression for v_{β}=0 that can be calculated from eqs 4−7.

$$\frac{(v - v_{[I]\to\infty})}{(v_0 - v_{[I]\to\infty})}v_0 = \frac{V_{max}[S]}{K_S\left(1+\frac{[I]}{K_i}\right) + [S]\left(1+\frac{[I]}{\alpha K_i}\right)} \quad (8)$$

Equation 8 allows for an easy access to the analysis of the data following the common Hanes−Woolf method, using the values v, v_0, $v_{[I]\to\infty}$, and [S] (eq 9).

$$\frac{(v_0 - v_{[I]\to\infty})[S]}{(v - v_{[I]\to\infty})v_0} = \frac{[S]}{V_{max}}\left(1+\frac{[I]}{\alpha K_i}\right) + \frac{K_S}{V_{max}}\left(1+\frac{[I]}{K_i}\right) \quad (9)$$

Replots of the slopes (eq 10) and intercepts (eq 11) of eq 9 versus [I] give values for αK_i and K_i; the value α can be calculated from the ratio of αK_i and K_i.

$$\text{slope} = \frac{1}{V_{max}\alpha K_i}[I] + \frac{1}{V_{max}} \quad (10)$$

$$\text{intercept} = \frac{K_S}{V_{max}K_i}[I] + \frac{K_S}{V_{max}} \quad (11)$$

The constant β is accessible via eq 3 and eq 7. Linearization of these equations according to the Hanes−Woolf plot give eq 12 and eq 13, respectively. The value of β can be calculated as the quotient of the slopes of eq 13 and eq 12.

$$\frac{[S]}{v_{[I]\to\infty}} = \frac{[S]}{\beta V_{max}} + \frac{\alpha K_S}{\beta V_{max}} \quad (12)$$

$$\frac{[S]}{v_0} = \frac{[S]}{V_{max}} + \frac{K_S}{V_{max}} \quad (13)$$

As noted above, most of the AChE inhibitors of the present series exhibited residual activity at infinite concentration. The rates $v_{[I]\to\infty}$, relative to v_0, are listed in Tables 1−4. From this it follows that β (Scheme 7) takes a value different from zero. To elucidate the enzyme−inhibitor interaction, it should be determined whether the inhibitor binds to the enzyme−substrate complex, ES; with a greater affinity than to the free enzyme, E, or vice versa. The preference of the inhibitor to bind to ES is reflected in values $\alpha < 1$ (Scheme 7) that indicate mixed type inhibition with a pronounced uncompetitive component. A higher affinity of the inhibitor to E, and thus values $\alpha > 1$, corresponds to mixed type inhibition with a more competitive character. Moreover, K_i values being independent of the substrate concentration should be made available.

Table 6. Kinetic Parameters for the Inhibition of AChE by Anticholinesterases

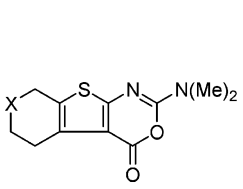

39, **40**

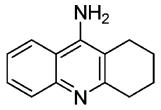

tacrine

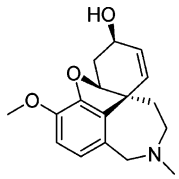

galanthamine

compd	X	IC_{50} (μM)	K_i (μM)	α	β
39	N-*i*-Bu	0.36 ± 0.01	0.66 ± 0.02	0.33	0.054
40	N-Bn	0.89 ± 0.02	1.70 ± 0.12	0.37	0.076
tacrine[a]	−	0.027 ± 0.001	0.025 ± 0.001	1.48	0
galanthamine[a]	−	2.20 ± 0.15	1.56 ± 0.07	4.82	0

[a] $v_{[I]\to\infty}$ was set to zero.

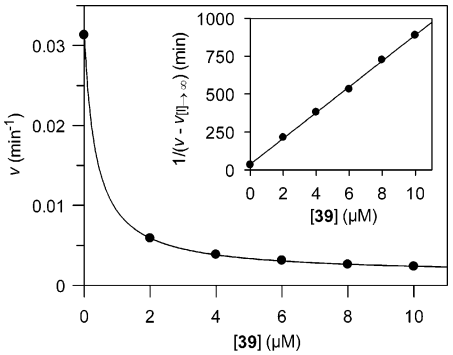

Figure 4. Inhibition of AChE by compound **39.** Plot of the rates versus [I] for the inhibition of AChE by compound **39** in 100 mM sodium phosphate, 100 mM NaCl, pH 7.3 with 350 μM DTNB, 6% acetonitrile, and 0.033 U/ml AChE. Initial substrate concentration was 500 μM ATCh. Rates were obtained by linear regression of the progress curves (not shown) and are mean values of duplicate experiments. A nonlinear regression according to eq 1, gave $IC_{50} = 0.36 \pm 0.01$ μM and $v_{[I]\to\infty} = 0.00134 \pm 0.00005$ min^{-1}, that corresponds to 0.043 ± 0.002 relative to v_0. The insert is a Dixon plot to show the linearity.

Actually, the kinetic analysis of the hyperbolic mixed-type inhibition of exemplary compounds was accomplished using the new methodology derived above. The basic thieno[1,3]oxazin-4-ones **39** and **40** as well as tacrine and galanthamine were selected (Table 6). The inhibition of AChE by the isobutyl derivative **39** is illustrated in Figure 4. An IC_{50} value of 360 nM and a relative residual activity $v_{[I]\to\infty}$ of 0.043 was obtained. Most of the active compounds gave similar plots, rate versus inhibitor concentration, and the parameters are noted in Tables 1−4. From observed residual activities $v_{[I]\to\infty}$ and thus β values different from zero, the occurrence of a ternary ESI complex could be predicted (Scheme 7). For those compounds, a purely competitive

type of inhibition and thus a relevant interaction with the esteratic site of AChE could be excluded.

Next, the dependence of the rates on the concentration of tacrine and galanthamine was analyzed. The nonlinear regression gave more accurate results when $v_{[I]\to\infty}$ was set to zero. It could therefore be concluded for both inhibitors, that the ESI complex, if formed at all, is not catalytically active. The further kinetic analysis for tacrine and galanthamine followed the model of linear mixed-type inhibition[80] with $\beta = 0$ (Scheme 7).

The determination of the factor α (Table 6) was performed to estimate the portion of competitive and uncompetitive inhibition, respectively. According to eq 9, a plot of $(v_0 - v_{[I]\to\infty})$ [S]/$((v - v_{[I]\to\infty})\, v_0)$ versus [S] and the respective secondary plots allow for the calculation of K_i and α. The procedure for compound **39** is depicted in Figures 5a and 5b, and was similarly applied to compound **40**. Values α = 0.33 and α = 0.37 for **39** and **40**, respectively, were obtained. In the case of tacrine and galanthamine, where $v_{[I]\to\infty}$ was set to zero, eq 9 can be simplified to that of the common Hanes–Woolf plot, [S]/v versus [S]. Corresponding analysis gave a factor α of 1.48 for tacrine and of 4.82 for galanthamine.

The factor β corresponds to the relative residual velocity $v_{[I]\to\infty}$ at infinite substrate concentration (eq 3), i.e. the ratio between the maximum velocity of the productive decay of ESI and ES (Scheme 7). The determination of factor β for compound **39** is illustrated in Figure 5c, showing the plots [S]/v_0 versus [S] and [S]/$v_{[I]\to\infty}$ versus [S]. Values of β for the inhibitors **39** and **40** (0.054 and 0.076, respectively) were obtained by linear regression according to eqs 12 and 13. The data $v_{[I]\to\infty}$ as noted in Table 3 are necessarily somewhat lower. Taken together, the two basic tetrahydropyrido derivatives **39** and **40** form ternary ESI complexes with a restricted catalytic efficiency. Their activity is less than 8% but still significant.

The α values indicated that both **39** and **40** are mixed-type inhibitors of AChE with a pronounced uncompetitive character (Table 6). The constant K_i that responds to competitive inhibition was calculated to be 0.66 μM (**39**) and 1.70 μM (**40**), respectively. The constant of the uncompetitive inhibition, αK_i, was 0.22 μM (**39**) and 0.63 μM (**40**), respectively. These parameters imply IC_{50} values between K_i and αK_i, closer to the latter value. This was indeed the case for inhibitors **39** and **40** (Table 6).

The α values for tacrine and galanthamine, on the other hand, demonstrate a pronounced competitive mode for tacrine (α = 1.48) that was even stronger in the case of galanthamine (α = 4.82). These findings were in agreement with literature data. On AChE from *Electrophorus electricus*, an α value of 1.88 (K_i = 20.4 nM) was determined for tacrine[85] and purely competitive inhibition (K_i = 660 nM) was reported for galanthamine.[86] The kinetic behavior reflects structural information derived from crystal structures of AChE complexed with tacrine[69] and galanthamine.[87,88] Both anticholinesterases occupied the anionic binding site stacking against the indole ring of Trp84 (*Torpedo californica* AChE numbering)[68] to form a favorable $\pi-\pi$ interaction. While galanthamine did not interact with Phe330, tacrine was sandwiched between the aromatic rings of Trp84 and Phe330 and additionally fixed through direct cation–π interactions on the residues of

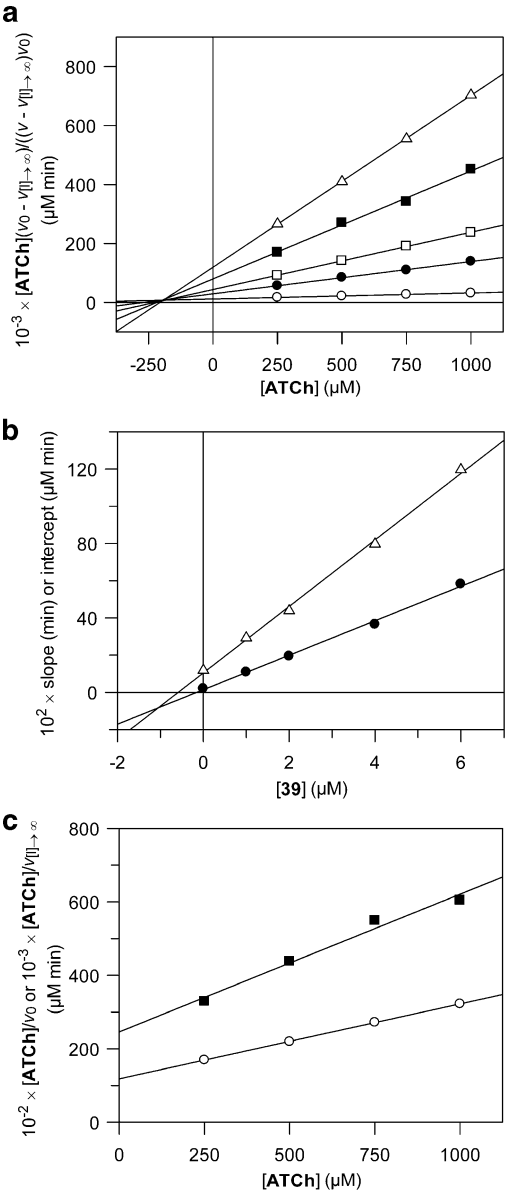

Figure 5. Inhibition of AChE by compound **39** in the presence of different concentrations of the substrate ATCh. (a) Modified Hanes–Woolf plot using mean values of rates from duplicate experiments in 100 mM sodium phosphate, 100 mM NaCl, pH 7.3 with 350 μM DTNB, 6% acetonitrile, and 0.033 U/mL AChE. Concentrations of compound **39** were as follows: open circles, [I] = 0; full circles, [I] = 1 μM; open squares, [I] = 2 μM; full squares, [I] = 4 μM; open triangles, [I] = 6 μM. Linear regression according to eq 9 gave values for slopes and vertical intercepts. (b) Plot of 10^2 × slopes (full circles) and vertical intercepts (open triangles) versus the concentrations of compound **39**. Linear regression according to eq 10 gave a slope $10^2/(\alpha K_i\, V_{max}) = 9.26 \pm 0.29\ \mu M^{-1}$ min, that corresponds to a value $\alpha K_i = 0.22 \pm 0.01\ \mu$M. Linear regression according to eq 11 gave a slope $K_m/(K_i\, V_{max}) = 17.9 \pm 0.5$ min, that corresponds to a value $K_i = 0.66 \pm 0.02\ \mu$M. The ratio of αK_i and K_i gave a value α = 0.33. (c) Hanes–Woolf plot using mean values of v_0 (open circles) and $v_{[I]\to\infty}$ (full squares) from duplicate experiments. Linear regression according to eq 13 gave a slope $10^{-2}/V_{max} = 0.204 \pm 0.002$ min for the plot 10^{-2} × [ATCh]/v_0 versus [ATCh], and a linear regression according to eq 12 gave a slope $10^{-3}/(\beta\, V_{max}) = 0.375 \pm 0.038$ min for the plot 10^{-3} × [ATCh]/$v_{[I]\to\infty}$ versus [ATCh]. Thus, a value β = 0.054 could be calculated.

the anionic binding site.[89] Tacrine did not occupy the immediate vicinity of the catalytic serine, whereas galanthamine participated in an hydrogen bond with the active site Ser200.[69,88] These arrangements provided some rationale for the stronger competitive behavior of galanthamine compared to tacrine.

The kinetic analyses as well as the structural similarities between known inhibitors and the pyridothieno-[1,3]oxazinones led us to suspect the orientation of our inhibitors in the active-site gorge of AChE. The benzyl-substituted tetrahydropyridine derivatives, being almost all active, resembled donepezil and AP2238[71] with respect to the benzyl substituent, its attachment to a basic nitrogen and the carbonyl group in a similar distance. The crystal structure of AChE (*Torpedo californica*) complexed with donepezil[90] showed the inhibitor oriented along the axis of the gorge, extending from the anionic site to the PAS. The interaction occurred via aromatic $\pi-\pi$ stacking between the benzyl moiety of donepezil and Trp84 as well as the indanone ring and Trp279. The charged piperidine nitrogen made a cation$-\pi$ interaction with Phe330 at the midpoint of the gorge. The carbonyl interacted with the aromatic rings of Phe331 and Phe290, and indirectly via a water molecule with the amide bond of Phe288. Donepezil did not directly interact with residues of the catalytic triad.[90] Similar contacts stabilized the complex of AP2238 with human AChE as concluded from docking studies. The coumarin ring interacted with the PAS and the carbonyl group established an H-bond interaction with a phenylalanine backbone amide group.[71] Both donepezil and AP2238 have been described as mixed-type inhibitors.[71,85] Noteworthy these substances excelled as inhibitors of the AChE-induced Aβ aggregation, a feature which was present only to a minor extent in the case of tacrine.[49,71]

It is tempting to assume that the benzyl-substituted tetrahydropyridine derivatives of our study (e.g. **40**) bind similarly to the active site gorge of AChE. An orientation toward the PAS and away from the esteratic site would be in accordance with the kinetic data of the enzyme−inhibitor interaction. In view of the structures of donepezil and AP2238, a dimethoxy phenyl moiety was introduced into the 2-substituent of our tricyclic skeleton to facilitate a contact to the PAS. The resulting derivative **21** proved to be the most potent AChE inhibitor of the present series.

Conclusions

Thirty six thieno[1,3]oxazin-4-ones and thieno[1,3]-thiazin-4-ones were evaluated in vitro as inhibitors of bovine pancreatic CEase as well as AChE from *Electrophorus electricus*, two members of the α/β-hydrolase family. Although the heterocyclic compounds of this series possess structural similarity, selective inhibitors of both esterases were identified. A crucial feature for specific interaction with AChE was the presence of a basic nitrogen in the ring fused to the thienoxazinone. When this moiety was excised or replaced by a methylene group, selectivity was reversed and inhibitors of CEase were attained, in principle, without further structural changes. The kinetic analyses revealed a generally different mode of inhibition toward the two target enzymes. In the case of CEase, the lactone unit of thienoxazinones served as an electrophile to mimic the scissile ester bond of substrates. Those compounds that underwent an enzyme-catalyzed steady-state hydrolysis were characterized as alternate substrate inhibitors. Kinetic parameters of the enzymatic turnover that assess the inhibitor's effectiveness are K_m and V_{max}, both with preferably low values. In this regard, the new inhibitor **33** meets the criteria of an efficient alternate substrate inhibitor of CEase. Moreover, **33** and its analogues are distinguished by high chemical stability.

On the other hand, in the case of AChE it was supposed that the lactone unit of thienoxazinones did not interact with the serine of the catalytic triad, and the inhibitors were oriented along the active site gorge. This assumption based on structural resemblance to known anticholinesterases and, more important, on the kinetic behavior of the active thienoxazinones. Catalytically competent ESI complexes with varying activities were detected and a stronger uncompetitive component was observed for selected compounds. To specify the parameters of inhibition, a new method was derived that let us kinetically characterize certain thieno[1,3]-oxazin-4-ones as hyperbolic mixed-type inhibitors of AChE. Structural modifications of the efficient inhibitor **21** are currently under investigation in our laboratories. Such approaches include the opening of the tetrahydropyridine ring to achieve a higher flexibility of the basic moiety.

Experimental Section

General Methods and Materials. Melting points were determined on a Gallenkamp capillary melting point apparatus and a Büchi 510 oil bath apparatus, and are not corrected. Compounds **6** and **44** were prepared using the Büchi Glas Uster autoclave 'TinyClave'. Thin-layer chromatography was performed on Merck aluminum sheets, silica gel 60 F_{254}. Preparative column chromatography was performed on Merck silica gel 60, 70−230 mesh. ^{13}C NMR spectra (125 MHz) and ^1H NMR spectra (500 MHz) were recorded on a Bruker Advance DRX 500 spectrometer in $CDCl_3$ at 25 °C or in DMSO-d_6 at 30 °C. ^{13}C NMR signals were assigned on the basis of DEPT-135 spectra and $^{13}C/^1H$ correlation experiments (HSQC). Chemical shifts (δ) are reported in ppm. Spin multiplicities are indicated by the following symbols: s (singlet), br s (broad singlet), d (doublet), br d (broad duplet), dd (doublet of doublet), t (triplet), br t (broad triplet), tt (triplet of triplet), q (quartet), sept (septet), and m (multiplet). IR spectra were measured with a Perkin-Elmer 1600 series FTIR spectrophotometer. Mass spectra (70 eV) were obtained on a MS-50 A.E.I. spectrometer under electron impact ionization (EI). Elemental analyses were performed with a Vario EL apparatus. UV spectra and spectrophotometric assays were done on a Varian Cary 50 Bio UV/vis spectrometer and a Varian Cary 100 Bio UV/vis spectrometer, both with a cell holder equipped with a constant temperature water bath. CEase from bovine pancreas (71.5 units/mg), ATCh, DTNB, sodium taurocholate (TC), pNPB, and tacrine hydrochloride hemihydrate were obtained from Sigma (Steinheim, Germany). AChE from *Electrophorus* electricus (1044 U/mg and 1276 U/mg) and anhydrous DMSO were purchased from Fluka (Deisenhofen, Germany). Galanthamine hydrobromide was from Calbiochem (Bad Soden, Germany). Compounds **26**,[38] **42**,[91] **43**,[76] **45**, **46**,[77] **52**, **53**, **55**, **56**, **58**−**60**,[39] **54**, **57**, and **61**−**63**[38] were prepared as described elsewhere. All ^1H NMR and ^{13}C NMR data can be found in the Supporting Information.

***tert*-Butyl 2-Amino-6-benzyl-4,5,6,7-tetrahydrothieno-[2,3-*c*]pyridine-3-carboxylate (1).** A mixture of *N*-benzyl-4-piperidone (9.46 g, 50 mmol), sulfur (1.6 g, 50 mmol), *tert*-butyl cyanoacetate (7.06 g, 50 mmol), and C_2H_5OH (25 mL) was treated dropwise with morpholine (4.35 g, 50 mmol) at

45 °C over 5 min. After being stirred for 5 h at 45 °C, the mixture was diluted with H_2O (200 mL) and extracted with ether (4 × 100 mL). The organic layer was washed with H_2O (4 × 50 mL) and dried (Na_2SO_4). The solvent was removed in vacuo, and the crude product was recrystallized from *n*-hexane to yield **1** (14.8 g, 86%) as yellowish crystals: mp 115−118 °C. Anal. ($C_{19}H_{24}N_2O_2S$) C, H, N.

***tert*-Butyl 6-Benzyl-4,5,6,7-tetrahydro-2-(3-isopropylureido)thieno[2,3-*c*]pyridine-3-carboxylate (2).** A mixture of **1** (6.89 g, 20 mmol), isopropyl isocyanate (3.92 g, 46 mmol), and dry pyridine (40 mL) was stirred at 70 °C for 66 h under argon atmosphere and kept at room temperature for 7 h. It was poured into ice−water (600 mL), and the precipitate was collected by filtration, washed with H_2O, dried, and recrystallized from CH_3OH to yield **2** (4.32 g, 49%) as yellowish crystals: mp 96−98 °C. Anal. ($C_{23}H_{31}N_3O_3S$ × 0.5 H_2O) C, H, N.

***tert*-Butyl 6-Benzyl-2-(3-cyclohexylureido)-4,5,6,7-tetrahydrothieno[2,3-*c*]pyridine-3-carboxylate (3).** A mixture of **1** (6.89 g, 20 mmol), cyclohexyl isocyanate (5.76 g, 46 mmol), and dry pyridine (40 mL) was stirred at 70 °C for 66 h under argon atmosphere, kept at room temperature for 7 h, and filtered. The filtrate was poured into ice−water (600 mL) and extracted with ethyl acetate (2 × 150 mL). The organic layer was washed with H_2O (2 × 300 mL) and dried (Na_2SO_4). The solvent was removed in vacuo, and the crude product was extracted with boiling *n*-hexane (3 × 300 mL). After cooling of the extractant, the precipitate was collected by filtration, combined with the residue of the extraction, and recrystallized from CH_3OH to yield **3** (5.56 g, 55%) as yellowish crystals: mp 106.5−108.5 °C. Anal. ($C_{26}H_{35}N_3O_3S$ × CH_3OH) C, H, N.

7-Benzyl-5,6,7,8-tetrahydro-2-isopropylamino-4*H*-pyrido[4′,3′:4,5]thieno[2,3-*d*][1,3]oxazin-4-one (4). A mixture of trifluoroacetic anhydride (1.47 g, 7 mmol) and trifluoroacetic acid (6 mL) was stirred at 0 °C under argon atmosphere. Compound **2** (2.15 g, 4.90 mmol) was added in portions over 30 min. Stirring was continued at 0 °C for 30 min and at room-temperature overnight. The mixture was poured into chilled saturated aqueous $NaHCO_3$ (100 mL). The precipitate was collected by filtration, washed with H_2O, and dried. The filtrate was extracted with ethyl acetate (2 × 100 mL). The organic layer was washed with H_2O (2 × 100 mL) and saturated aqueous NaCl (100 mL) and dried (Na_2SO_4). After removal of the solvent in vacuo, the residue was combined with the precipitate and recrystallized twice from ethyl acetate/*n*-hexane (3:4) with the addition of silica gel (8.5 g) to yield **4** (0.47 g, 27%) as a white solid: mp 192−193 °C (decomp); HRMS *m/z* calcd for $C_{19}H_{20}N_3O_2S$ ($M^+ - H$), 354.1276; found, 354.1276. Anal. ($C_{19}H_{21}N_3O_2S$ × 0.25 H_2O) C, H, N.

7-Benzyl-2-cyclohexylamino-5,6,7,8-tetrahydro-4*H*-pyrido[4′,3′:4,5]thieno[2,3-*d*][1,3]oxazin-4-one (5). According to the procedure outlined above, **3** (2.35 g, 4.68 mmol) was used in place of **2**. The mixture was poured into chilled saturated aqueous $NaHCO_3$ (120 mL). The precipitate was collected by filtration, washed with H_2O, and dried. Boiling ethyl acetate (400 mL) and silica gel (23 g) were added, and the mixture was refluxed and filtered. After adding *n*-hexane (300 mL) and silica gel (19 g) to the filtrate, it was refluxed and filtered. The solvent was removed in vacuo, and the residue was recrystallized from ethyl acetate/*n*-hexane (2:3) with the addition of silica gel (7.5 g) to yield **5** (0.15 g, 8%) as a white solid: mp 189−192 °C (decomp); HRMS *m/z* calcd for $C_{22}H_{24}N_3O_2S$ ($M^+ - H$), 394.1589; found, 394.1585. Anal. ($C_{19}H_{21}N_3O_2S$ × 0.5 H_2O) C, H, N.

***tert*-Butyl 6-Benzyl-4,5,6,7-tetrahydro-2-(3-phenylthioureido)thieno[2,3-*c*]pyridine-3-carboxylate (6).** A mixture of **1** (3.44 g, 10 mmol), phenyl isothiocyanate (3.79 g, 28 mmol), and dry C_2H_5OH (4 mL) was stirred in an autoclave at 80 °C for 1.5 h under argon atmosphere. After keeping the reaction mixture at room-temperature overnight, the precipitate was collected by filtration, washed with cold C_2H_5OH, and dried to obtain **6** (4.52 g, 94%) as a yellowish solid: mp 190−191 °C (decomp). Anal. ($C_{26}H_{29}N_3O_2S_2$) C, H, N.

7-Benzyl-5,6,7,8-tetrahydro-2-phenylamino-4*H*-pyrido[4′,3′:4,5]thieno[2,3-*d*][1,3]oxazin-4-one (7). Compound **6** (2.40 g, 5 mmol) was added in portions over 20 min to trifluoroacetic acid (7 mL) at 0 °C. After being stirred for additional 30 min at 0 °C and for 1.5 h at room temperature, the mixture was poured into chilled saturated aqueous $NaHCO_3$ (120 mL). The precipitate was collected by filtration, washed with H_2O, and dried to obtain a yellowish solid (3.14 g). It was dissolved in boiling dry CH_2Cl_2 (150 mL), cooled to room temperature, and filtered. After adding yellow HgO (2.56 g, 11.80 mmol) to the filtrate, the mixture was stirred at room temperature for 48 h. Silica gel (5.3 g) was added and the mixture was stirred for 2 min. The inorganic material was filtered off and washed with dry CH_2Cl_2 (75 mL). The wash was combined with the filtrate, and the solvent was removed in vacuo to yield **7** (0.34 g, 16%) as a yellowish solid: mp 196−197 °C (ethyl acetate/*n*-hexane, 1:4, decomp); HRMS *m/z* calcd for $C_{22}H_{18}N_3O_2S$ ($M^+ - H$), 388.1120; found, 388.1129. Anal. ($C_{22}H_{19}N_3O_2S$ × 0.3 $CH_3COOC_2H_5$) C, H, N.

2-Benzoylamino-7-benzyl-5,6,7,8-tetrahydro-4*H*-pyrido[4′,3′:4,5]thieno[2,3-*d*][1,3]oxazin-4-one (8). Ammonium thiocyanate (1.00 g, 13.10 mmol) was dissolved in boiling dry CH_3COCH_3 (8 mL), filtered, and cooled to 0 °C. After dropwise addition of benzoyl chloride (1.63 g, 11.6 mmol), the mixture was refluxed for 5 min. The precipitate was filtered off and washed with dry CH_3COCH_3 (6 mL). The filtrate and the wash were combined and added to a solution of **1** (2.00 g, 5.80 mmol) in dry CH_3COCH_3 (12 mL). After being stirred for 2 h at room temperature, the precipitate was collected by filtration, washed with cold CH_3COCH_3, and dried to obtain a yellowish solid (2.54 g). It was added in portions over 20 min to trifluoroacetic acid (6 mL) at 0 °C. After being stirred for additional 40 min at 0 °C and for 2 h at room temperature, the mixture was poured into chilled saturated aqueous $NaHCO_3$ (100 mL). The precipitate was collected by filtration, washed with H_2O, and dried to obtain a yellowish solid (2.54 g). It was dissolved in dry CH_2Cl_2 (110 mL), yellow HgO (1.95 g, 9 mmol) was added, and the mixture was stirred at room temperature for 48 h. Silica gel (4 g) was added and the mixture was stirred for 2 min. The inorganic material was filtered off and washed with dry CH_2Cl_2 (55 mL). After combination of the wash with the filtrate and the removal of the solvent in vacuo, the residue was recrystallized from ethyl acetate/*n*-hexane (1:2) to yield **8** (0.18 g, 7%) as a yellowish solid: mp 143−146 °C (decomp); HRMS *m/z* calcd for $C_{23}H_{18}N_3O_3S$ ($M^+ - H$), 416.1069; found, 416.1075. Anal. ($C_{23}H_{19}N_3O_3S$) C, H, N.

***tert*-Butyl 6-Benzyl-2-(3-trichloroacetylureido)-4,5,6,7-tetrahydrothieno[2,3-*c*]pyridine-3-carboxylate (9).** Compound **1** (3.44 g, 10 mmol) was dissolved in dry THF (15 mL) and the solution was cooled to 0 °C. After adding cold trichloroacetyl isocyanate (4.33 g, 23 mmol), the reaction mixture was stirred at 0 °C for 30 min and at 7−10 °C for 2.5 h under argon atmosphere. Purification by column chromatography (petrol ether/ethyl acetate, 2:1, performed at 8 °C) and removal of the solvent in vacuo at 7−10 °C yielded **9** (4.77 g, 90%) as a greenish solid: mp 179−182 °C (decomp).

***tert*-Butyl 6-Benzyl-4,5,6,7-tetrahydro-2-ureidothieno[2,3-*c*]pyridine-3-carboxylate (10).** Compound **9** (10.21 g, 19.16 mmol) was dissolved in a mixture of dry CH_3OH (25 mL) and dry THF (25 mL) and the solution was stirred at 60 °C for 5.5 h. After removal of the solvent in vacuo the crude product was recrystallized from CH_3OH to obtain **10** (2.37 g, 32%) as yellowish crystals: mp 224−225 °C (decomp). Anal. ($C_{20}H_{25}N_3O_3S$) C, H, N.

6-Benzyl-3-carboxy-4,5,6,7-tetrahydro-2-ureidothieno[2,3-*c*]pyridin-6-ium Trifluoroacetate (11). Compound **10** (1.16 g, 3 mmol) was added in portions over 30 min to trifluoroacetic acid (4 mL) at 0 °C under argon atmosphere. After being stirred in an open flask equipped with a drying tube at room temperature for additional 1.5 h, the trifluoroacetic acid was removed in vacuo at room temperature. The residue was dissolved in dry CH_2Cl_2 (5 mL) and *n*-hexane (5 mL) was added to obtain an oily precipitate. After keeping at −18 °C for 4 days, the precipitate was consolidated. It was

collected by filtration, washed with *n*-hexane, and dried to obtain **11** (1.61 g, 84%) as a white solid: mp 153−156 °C (decomp). Anal. ($C_{16}H_{17}N_3O_3S \times 2.7\ CF_3COOH$) C, H, N.

2-Amino-7-benzyl-5,6,7,8-tetrahydro-4*H*-pyrido[4′,3′:4,5]thieno[2,3-*d*][1,3]oxazin-4-one (12). Compound **11** (0.8 g, 1.25 mmol) was dissolved in trifluoroacetic acid (4 mL) and stirred at 0 °C under argon atmosphere. A solution of trifluoroacetic anhydride (0.38 g, 1.79 mmol) in trifluoroacetic acid (2 mL) was added dropwise over 15 min. Stirring was continued at 0 °C for 1 h and at room-temperature overnight. The trifluoroacetic acid and the trifluoroacetic anhydride were removed in vacuo at room temperature. The residue was dissolved in dry CH_2Cl_2 (4 mL), and *n*-hexane (4 mL) was added to obtain an oily precipitate. After keeping at −18 °C for 6 days, the precipitate was consolidated. It was collected by filtration, washed with *n*-hexane, and dried. The crude product was dissolved in a mixture of CH_3OH (60 mL) and ice−water (180 mL) and filtered. The acidic filtrate (pH 3−4) was adjusted to pH 7 by dropwise addition of saturated aqueous $NaHCO_3$. The precipitate was collected by filtration, washed with cold H_2O, and dried to obtain **12** (0.21 g, 51%) as a yellowish solid: mp 184.5−185 °C (decomp); HRMS *m/z* calcd for $C_{16}H_{14}N_3O_2S$ ($M^+ - H$), 312.0807; found, 312.0803. Anal. ($C_{16}H_{15}N_3O_2S \times 0.7\ H_2O$) C, H, N.

6-Benzyl-3-*tert*-butoxycarbonyl-4,5,6,7-tetrahydro-2-(4-nitrophenoxycarbonylamino)thieno[2,3-*c*]pyridin-6-ium Chloride (13). A mixture of **1** (4.13 g, 12 mmol), dry pyridine (1.66 g, 21 mmol), and dry $Cl(CH_2)_2Cl$ (150 mL) was stirred at 0 °C. A solution of *p*-nitrophenyl chloroformate (2.58 g, 12.8 mmol) in dry $Cl(CH_2)_2Cl$ (15 mL) was added dropwise over 35 min. After being stirred at 0 °C for 1.5 h, the reaction mixture was kept at −18 °C overnight. The precipitate was collected by filtration, washed with dry CH_2Cl_2, and dried to obtain **13** (3.82 g, 56%) as white crystals: mp 169−172 °C (decomp). Anal. ($C_{26}H_{27}N_3O_6S \times HCl \times 0.25\ CH_2Cl_2$) C, H, N.

***tert*-Butyl 6-Benzyl-2-(3,3-diethylureido)-4,5,6,7-tetrahydrothieno[2,3-*c*]pyridine-3-carboxylate (14).** Compound **13** (3.28 g, 5.78 mmol) was suspended in dry $Cl(CH_2)_2Cl$ (90 mL) and stirred at 0 °C under argon atmosphere. A solution of diethylamine (1.54 g, 21 mmol) in dry $Cl(CH_2)_2Cl$ (15 mL) was added dropwise over 20 min. After being stirred at 0 °C for 30 min, the reaction mixture was diluted with $Cl(CH_2)_2Cl$ (100 mL), washed with H_2O (5 × 300 mL) and saturated aqueous NaCl (300 mL), and dried (Na_2SO_4). The solvent was removed in vacuo, and the crude product was recrystallized from CH_3OH to yield **14** (1.46 g, 56%) as dark yellow crystals: mp 141−143 °C. Anal. ($C_{24}H_{33}N_3O_3S \times 0.25\ CH_3OH$) C, H, N.

***tert*-Butyl 6-Benzyl-2-(3-benzyl-3-methylureido)-4,5,6,7-tetrahydrothieno[2,3-*c*]pyridine-3-carboxylate (15).** Compound **13** (2.84 g, 5 mmol) was suspended in dry $Cl(CH_2)_2Cl$ (70 mL) and stirred at 0 °C under argon atmosphere. A solution of *N*-benzyl-*N*-methylamine (4.24 g, 35 mmol) in dry $Cl(CH_2)_2Cl$ (30 mL) was added dropwise over 20 min. After being stirred at 0 °C for 1.5 h and at room temperature for additional 1.5 h, the reaction mixture was kept at − 18 °C overnight. The precipitate was filtered off and washed with dry $Cl(CH_2)_2Cl$ (80 mL). After combination of the organic layers, they were washed with H_2O (7 × 200 mL) and saturated aqueous NaCl (200 mL) and dried (Na_2SO_4). The solvent was removed in vacuo, and the crude product was recrystallized from CH_3OH to yield **15** (1.64 g, 67%) as yellow crystals: mp 153−154 °C. Anal. ($C_{28}H_{33}N_3O_3S$) C, H, N.

***tert*-Butyl 6-Benzyl-2-[3-(3,4-dimethoxybenzyl)-3-methylureido]-4,5,6,7-tetrahydrothieno[2,3-*c*]pyridine-3-carboxylate (16).** Compound **13** (2.27 g, 4 mmol) was suspended in dry $Cl(CH_2)_2Cl$ (60 mL) and stirred at 0 °C under argon atmosphere. A solution of *N*-(3,4-dimethoxybenzyl)-*N*-methylamine (2.34 g, 14 mmol) in dry $Cl(CH_2)_2Cl$ (10 mL) was added dropwise over 20 min. After being stirred at 0 °C for 1.5 h and at room temperature for 1 h, the precipitate was filtered off and washed with dry $Cl(CH_2)_2Cl$ (80 mL). After combination of the organic layers, they were washed with H_2O (7 × 200 mL) and saturated aqueous NaCl (200 mL) and dried (Na_2SO_4). The solvent was removed in vacuo, and the crude product was recrystallized from CH_3OH to yield **16** (1.31 g, 60%) as yellow crystals: mp 141−142 °C. Anal. ($C_{30}H_{37}N_3O_5S$) C, H, N.

***tert*-Butyl 6-Benzyl-4,5,6,7-tetrahydro-2-[(4-morpholinylcarbonyl)amino]thieno[2,3-*c*]pyridine-3-carboxylate (17).** Compound **13** (2.18, 3.84 mmol) was suspended in dry $Cl(CH_2)_2Cl$ (100 mL) and stirred at 0 °C under argon atmosphere. A solution of morpholine (3.66 g, 42 mmol) in dry $Cl(CH_2)_2Cl$ (20 mL) was added dropwise over 30 min. After being stirred at 0 °C for 2 h and at room temperature for 1.5 h, the reaction mixture was washed with H_2O (5 × 200 mL) and saturated aqueous NaCl (100 mL) and dried (Na_2SO_4). The solvent was removed in vacuo, and the crude product was recrystallized from CH_3OH to yield **17** (1.37 g, 78%) as yellow crystals: mp 204.5−207.5 °C (decomp). Anal. ($C_{24}H_{31}N_3O_4S$) C, H, N.

***tert*-Butyl 6-Benzyl-2-[(4-benzyl-1-piperazinylcarbonyl)amino]-4,5,6,7-tetrahydrothieno[2,3-*c*]pyridine-3-carboxylate (18).** Compound **13** (2.18 g, 3.84 mmol) was suspended in dry $Cl(CH_2)_2Cl$ (60 mL) and stirred at 0 °C under argon atmosphere. A solution of 1-benzylpiperazine (2.47 g, 14 mmol) in dry $Cl(CH_2)_2Cl$ (10 mL) was added dropwise over 10 min. After being stirred at 0 °C for 1.5 h, the reaction mixture was diluted with $Cl(CH_2)_2Cl$ (40 mL), washed with H_2O (6 × 200 mL) and saturated aqueous NaCl (200 mL) and dried (Na_2SO_4). The solvent was removed in vacuo, and the crude product was recrystallized from CH_3OH to yield **18** (1.41 g, 66%) as yellowish crystals: mp 127.5−129.5 °C. Anal. ($C_{31}H_{38}N_4O_3S \times 0.35\ CH_3OH$) C, N; H: calcd, 7.12, found, 6.71.

7-Benzyl-2-diethylamino-5,6,7,8-tetrahydro-4*H*-pyrido[4′,3′:4,5]thieno[2,3-*d*][1,3]oxazin-4-one (19). A mixture of trifluoroacetic anhydride (0.88 g, 4.2 mmol) and trifluoroacetic acid (3 mL) was stirred at 0 °C under argon atmosphere. Compound **14** (1.33 g, 2.95 mmol) was added in portions over 30 min. Stirring was continued at 0 °C for 30 min and at room-temperature overnight. The mixture was poured into chilled saturated aqueous $NaHCO_3$ (70 mL) and extracted with ethyl acetate (2 × 100 mL). The organic layer was washed with H_2O (2 × 50 mL) and saturated aqueous NaCl (50 mL) and dried (Na_2SO_4). After removal of the solvent in vacuo, the residue was recrystallized from *n*-hexane to yield **19** (0.86 g, 79%) in two modifications, as yellow crystals and a yellow solid, which were combined: mp 116−117 °C; HRMS *m/z* calcd for $C_{20}H_{22}N_3O_2S$ ($M^+ - H$), 368.1433; found, 368.1441. Anal. ($C_{20}H_{23}N_3O_2S$) C, H, N.

7-Benzyl-2-(*N*-benzyl-*N*-methylamino)-5,6,7,8-tetrahydro-4*H*-pyrido[4′,3′:4,5]thieno[2,3-*d*][1,3]oxazin-4-one (20). A mixture of trifluoroacetic anhydride (0.59 g, 2.80 mmol) and trifluoroacetic acid (3.5 mL) was stirred at 0 °C under argon atmosphere. Compound **15** (0.98 g, 2 mmol) was added in portions over 30 min. Stirring was continued at 0 °C for 30 min and at room-temperature overnight. The mixture was poured into chilled saturated aqueous $NaHCO_3$ (90 mL) and extracted with ethyl acetate (2 × 100 mL). The organic layer was washed with H_2O (2 × 50 mL) and saturated aqueous NaCl (50 mL) and dried (Na_2SO_4). After removal of the solvent in vacuo, the residue was recrystallized from *n*-hexane to yield **20** (0.63 g, 75%) as a white solid: mp 156−158 °C; HRMS *m/z* calcd for $C_{24}H_{22}N_3O_2S$ ($M^+ - H$), 416.1433; found, 416.1434. Anal. ($C_{24}H_{23}N_3O_2S \times 0.25\ H_2O$) C, H, N.

7-Benzyl-5,6,7,8-tetrahydro-2-(*N*-3,4-dimethoxybenzyl-*N*-methylamino)-4*H*-pyrido[4′,3′:4,5]thieno[2,3-*d*][1,3]-oxazin-4-one (21). Compound **16** (1.10 g, 2 mmol) was added in portions over 30 min to trifluoroacetic acid (3 mL), which was stirred at 0 °C under argon atmosphere. After being stirred for additional 2 h at 0 °C, the mixture was washed with cold *n*-hexane (2 × 5 mL) and a cold mixture of dry CH_2Cl_2 (20 mL) and *n*-hexane (30 mL). The oily residue was dried in vacuo, dissolved in dry CH_2Cl_2 (2 mL), and stirred at 0 °C under argon atmosphere. A solution of trifluoroacetic anhydride (0.59 g, 2.80 mmol) in dry CH_2Cl_2 (4 mL) was added dropwise over 15 min. Stirring was continued at 0 °C for 1 h, and the reaction mixture was kept at 4 °C overnight. After

drying in vacuo, the residue was dissolved in cold CH_3OH (30 mL) and poured into ice−water (60 mL). The mixture (pH 2−3) was adjusted to pH 8 by dropwise addition of saturated aqueous $NaHCO_3$. The precipitate was collected by filtration, washed with water, dried, and purified by column chromatography (CH_2Cl_2/ethyl acetate, 4:1) followed by recrystallization from ethyl acetate/*n*-hexane (1:9) to yield **21** (0.08 g, 8%) as a yellowish solid: mp 157−159 °C (decomp, crystal conversion to yellow crystals at 120 °C); HRMS *m/z* calcd for $C_{26}H_{26}N_3O_4S$ ($M^+ - H$), 476.1644; found, 476.1638. Anal. ($C_{26}H_{27}N_3O_4S \times 0.75\ H_2O$) C, H, N.

7-Benzyl-5,6,7,8-tetrahydro-2-(morpholin-4-yl)-4*H*-pyrido[4′,3′:4,5]thieno[2,3-*d*][1,3]oxazin-4-one (22). A mixture of trifluoroacetic anhydride (0.59 g, 2.8 mmol) and trifluoroacetic acid (2 mL) was stirred at 0 °C under argon atmosphere. Compound **17** (0.92 g, 2 mmol) was added in portions over 30 min. Stirring was continued at 0 °C for 30 min and at room-temperature overnight. The mixture was poured into chilled saturated aqueous $NaHCO_3$ (50 mL) and extracted with ethyl acetate (2 × 200 mL). The organic layer was washed with H_2O (2 × 100 mL) and saturated aqueous NaCl (100 mL) and dried (Na_2SO_4). After removal of the solvent in vacuo, the residue was recrystallized from *n*-hexane to yield **22** (0.25 g, 33%) as yellow crystals: mp 154−155.5 °C; HRMS *m/z* calcd for $C_{20}H_{20}N_3O_3S$ ($M^+ - H$), 382.1225; found, 382.1229. Anal. ($C_{20}H_{21}N_3O_3S$) C, H, N.

7-Benzyl-2-(4-benzylpiperazin-1-yl)-5,6,7,8-tetrahydro-4*H*-pyrido[4′,3′:4,5]thieno[2,3-*d*][1,3]oxazin-4-one (23). A mixture of trifluoroacetic anhydride (0.59 g, 2.8 mmol) and trifluoroacetic acid (3 mL) was stirred at 0 °C under argon atmosphere. Compound **18** (1.09 g, 1.96 mmol) was added in portions over 1 h. Stirring was continued at 0 °C for 30 min and at room-temperature overnight. The mixture was poured into chilled saturated aqueous $NaHCO_3$ (70 mL) and extracted with ethyl acetate (2 × 100 mL). Insoluble material was filtered off and washed with ethyl acetate (2 × 50 mL). After combination of the organic layers, they were washed with H_2O (2 × 100 mL) and saturated aqueous NaCl (100 mL) and dried (Na_2SO_4). The solvent was removed in vacuo, and the residue was recrystallized from *n*-hexane to yield **23** (0.07 g, 8%) as yellow crystals: mp 149−150.5 °C; HRMS *m/z* calcd for $C_{27}H_{27}N_4O_2S$ ($M^+ - H$), 471.1885; found, 471.1885. Anal. ($C_{27}H_{28}N_4O_2S \times 0.25\ H_2O$) C, H, N.

***tert*-Butyl α-Cyano-α-cyclopentylidene-acetate (24).** Following a similar methodology,[92] cyclopentanone (18.8 g, 224 mmol) and *tert*-butyl cyanoacetate (25.3 g, 179 mmol) were dissolved in dry toluene. Glacial acetic acid (3.00 g, 50 mmol) and ammonium acetate (2.00 g, 26 mmol) were added, and the mixture was refluxed for 15 h using a Dean−Stark water trap. After cooling, the reaction mixture was washed with half-saturated aqueous NaCl (4 × 30 mL) and dried (Na_2SO_4). The volume was reduced in vacuo, and the mixture was kept at −72 °C. The precipitate was collected by filtration to obtain **24** (16.2 g, 44%) as brownish crystals: mp 93−94 °C (C_2H_5OH), lit. mp 87−88 °C.[93] Anal. ($C_{12}H_{17}NO_2 \times 0.1\ C_2H_5OH$) C, H, N.

***tert*-Butyl 2-Amino-5,6-dihydro-4*H*-cyclopenta[*b*]-thiophene-3-carboxylate (25).** A mixture of compound **24** (4.15 g, 20 mmol), sulfur (0.64 g, 20 mmol), and C_2H_5OH (25 mL) was treated dropwise with diethylamine (1.46 g, 20 mmol) at 60 °C over 5 min. After being stirred for 10 h at 60 °C, and 84 h at room temperature, the mixture was diluted with 0.4 M acetic acid (120 mL) and extracted with ether (1 × 75 mL and 4 × 30 mL). The organic layer was washed with H_2O (4 × 20 mL), dried (Na_2SO_4), and the solvent was removed in vacuo. The crude product was purified by 2-fold column chromatography (petrol ether/ethyl acetate, 10:1) to yield **25** (2.05 g, 43%) as yellow crystals: mp 68−72 °C. Anal. ($C_{12}H_{17}NO_2S$) C, H, N.

***tert*-Butyl 2-Amino-4,7-dihydro-5*H*-thieno[2,3-*c*]pyran-3-carboxylate (27).** A mixture of tetrahydropyran-4-one (0.90 g, 9 mmol), sulfur (0.29 g, 9 mmol), *tert*-butyl cyanoacetate (1.27 g, 9 mmol), and C_2H_5OH (10 mL) was treated dropwise with morpholine (0.78 g, 9 mmol) at 65 °C over 5 min. After being stirred for 5 h at 65 °C, the mixture was diluted with 0.4 M acetic acid (80 mL) and extracted with ether (1 × 65 mL and 3 × 15 mL). The organic layer was washed with H_2O (3 × 20 mL) and dried (Na_2SO_4). The solvent was removed in vacuo, and the crude product was recrystallized from *n*-hexane to yield **27** (1.98 g, 86%) as yellow crystals: mp 95−96 °C. Anal. ($C_{12}H_{17}NO_3S$) C, H, N.

***tert*-Butyl 2-Amino-4,7-dihydro-5*H*-thieno[2,3-*c*]thiopyran-3-carboxylate (28).** A mixture of tetrahydrothiopyran-4-one (0.93 g, 8 mmol), sulfur (0.26 g, 8 mmol), *tert*-butyl cyanoacetate (1.13 g, 8 mmol), and C_2H_5OH (10 mL) was treated dropwise with morpholine (0.70 g, 8 mmol) at 60 °C over 5 min. After being stirred for 5 h at 60 °C, the mixture was diluted with 0.4 M acetic acid (80 mL) and extracted with ether (1 × 65 mL and 3 × 15 mL). The organic layer was washed with H_2O (3 × 20 mL) and dried (Na_2SO_4). The solvent was removed in vacuo, and the crude product was recrystallized from *n*-hexane to yield **28** (1.60 g, 74%) as yellowish crystals: mp 91−93 °C. Anal. ($C_{12}H_{17}NO_2S_2$) H, N; C: calcd, 53.11; found, 53.59.

***tert*-Butyl 2-Amino-4,5,6,7-tetrahydro-6-methylthieno-[2,3-*c*]pyridine-3-carboxylate (29).** A mixture of *N*-methyl-4-piperidone (1.13 g, 10 mmol), sulfur (0.32 g, 10 mmol), *tert*-butyl cyanoacetate (1.41 g, 10 mmol), and C_2H_5OH (10 mL) was treated dropwise with morpholine (0.87 g, 10 mmol) at 45 °C over 5 min. After being stirred for 5 h at 45 °C, the mixture was diluted with H_2O (30 mL) and extracted with ether (1 × 65 mL and 4 × 15 mL). The organic layer was washed with H_2O (3 × 20 mL) and dried (Na_2SO_4). The solvent was removed in vacuo, and the crude product was recrystallized from *n*-hexane to yield **29** (2.1 g, 78%) as yellowish crystals: mp 134 °C. Anal. ($C_{13}H_{20}N_2O_2S$) C, H, N.

***tert*-Butyl 2-Amino-6-ethyl-4,5,6,7-tetrahydrothieno-[2,3-*c*]pyridine-3-carboxylate (30).** Compound **30** was prepared by the foregoing procedure, but using *N*-ethyl-4-piperidone (1.27 g, 10 mmol) in place of *N*-methyl-4-piperidone. The crude product was recrystallized from *n*-hexane to yield **30** (1.7 g, 60%) as yellow crystals: mp 74 °C. Anal. ($C_{14}H_{22}N_2O_2S$) C, H, N.

***tert*-Butyl 2-Amino-4,5,6,7-tetrahydro-6-(2-methylpropyl)thieno[2,3-*c*]pyridine-3-carboxylate (31).** According to the procedure outlined above, *N*-(2-methylpropyl)-4-piperidone (1.55 g, 10 mmol) was used in place of *N*-methyl-4-piperidone. The crude product was dissolved in boiling *n*-hexane and filtered. Removal of the solvent in vacuo yielded **31** (2.94 g, 95%) as a bay oil. A sample for elemental analysis was prepared by dissolving **31** in dry $Cl(CH_2)_2Cl$, adding 4 M HCl solution in 1,4-dioxane, and ether. The mixture was kept at −18 °C and the hydrochloride of **31** was filtered off (mp > 120 °C, decomp). Anal. ($C_{16}H_{26}N_2O_2S \times 1.4\ HCl$) C, H, N.

***tert*-Butyl 2-Amino-6-benzoyl-4,5,6,7-tetrahydrothieno-[2,3-*c*]pyridine-3-carboxylate (32).** A mixture of *N*-benzoyl-4-piperidone (0.55 g, 2.7 mmol), sulfur (0.09 g, 2.7 mmol), *tert*-butyl cyanoacetate (0.38 g, 2.7 mmol), and C_2H_5OH (30 mL) was treated dropwise with morpholine (0.24 g, 2.7 mmol) at 45 °C over 5 min. After being stirred for 15 h at 45 °C, the white precipitate was collected by filtration. The filtrate was diluted with H_2O (30 mL) and extracted with ether (1 × 70 mL and 2 × 15 mL). The organic layer was washed with H_2O (2 × 50 mL) and dried (Na_2SO_4). The solvent was removed in vacuo to obtain an additional amount of **32** (total yield 0.82 g, 82%): mp 210−217 °C (decomp). Anal. ($C_{19}H_{22}N_2O_3S$) C, H, N.

6,7-Dihydro-2-(dimethylamino)-4*H*,5*H*-cyclopenta[4,5]-thieno[2,3-*d*][1,3]oxazin-4-one (33). Compound **25** (1.00 g, 4.18 mmol) was dissolved in dry $Cl(CH_2)_2Cl$ (15 mL), and dichloromethylene dimethylammonium chloride (0.68 g, 4.18 mmol) was added. After being stirred for 5 min at room temperature, the reaction mixture was cooled to 0 °C, treated with 1 M ethereal HCl (0.9 mL), and refluxed for 1 h. After cooling, the precipitate was collected by filtration, washed with cold $Cl(CH_2)_2Cl$, and dried. The crude product was recrystallized from *n*-hexane to yield **33** (0.44 g, 45%) as white

crystals: mp 143−144 °C; HRMS *m/z* calcd for $C_{11}H_{12}N_2O_2S$ (M^+), 236.0620; found, 236.0616. Anal. ($C_{11}H_{12}N_2O_2S$) C, H, N.

5,6,7,8-Tetrahydro-2-(dimethylamino)-4*H*-benzo[4,5]-thieno[2,3-*d*][1,3]oxazin-4-one (34). Compound **26** (1.00 g, 9 mmol) was dissolved in dry $Cl(CH_2)_2Cl$ (25 mL), and dichloromethylene dimethylammonium chloride (1.46 g, 9 mmol) was added. The reaction mixture was cooled to 0 °C, treated with 1 M ethereal HCl (1.8 mL), and refluxed for 1 h. After cooling, the precipitate was collected by filtration, washed with cold $Cl(CH_2)_2Cl$, and dried to obtain **34** × **HCl** (0.72 g, 43%). An analytical sample was obtained by recrystallization from 50% C_2H_5OH to yield **34** as a white solid: mp 165−166 °C, lit. mp 156−157 °C;[75] HRMS *m/z* calcd for $C_{12}H_{14}N_2O_2S$ (M^+), 250.0776; found, 250.0778. Anal. ($C_{12}H_{14}N_2O_2S$ × HCl) C, H, N.

5,8-Dihydro-2-(dimethylamino)-4*H*,6*H*-pyrano[4′,3′:4,5]-thieno[2,3-*d*][1,3]oxazin-4-one (35). Compound **27** (1.28 g, 5 mmol) was dissolved in dry $Cl(CH_2)_2Cl$ (30 mL), and dichloromethylene dimethylammonium chloride (0.81 g, 5 mmol) was added. After being stirred for 30 min at 50 °C, the reaction mixture was cooled to 0 °C, treated with 1 M ethereal HCl (1.8 mL), and refluxed for 1 h. After removal of the solvent in vacuo, the residue was treated with boiling *n*-hexane (250 mL). The suspension was refluxed for 30 min and filtered. The filtrate was cooled and the precipitate was collected by filtration to obtain **35** (0.25 g, 20%) as white crystals: mp 194−196 °C (decomp); HRMS *m/z* calcd for $C_{11}H_{12}N_2O_3S$ (M^+), 252.0569; found, 252.0572. Anal. ($C_{11}H_{12}N_2O_3S$) H, N; C: calcd, 52.37; found, 52.93.

2-Dimethylamino-5,8-dihydro-4*H*,6*H*-thiopyrano[4′,3′:4,5]thieno[2,3-*d*][1,3]oxazin-4-one (36). Compound **28** (1.36 g, 5 mmol) was dissolved in dry $Cl(CH_2)_2Cl$ (15 mL), and dichloromethylene dimethylammonium chloride (0.81 g, 5 mmol) was added. After being stirred for 15 min at room temperature, the reaction mixture was cooled to 0 °C, treated with 1 M ethereal HCl (1.1 mL), and refluxed for 1 h. After keeping the reaction mixture for 45 min at 4 °C, the precipitate was collected by filtration, washed with cold $Cl(CH_2)_2Cl$, and dried. The crude product was treated with boiling *n*-hexane (100 mL). The suspension was refluxed for 40 min and filtered. The filtrate was cooled and the precipitate was collected by filtration to obtain **36** (0.64 g, 48%) as white crystals: mp 174−175 °C; HRMS *m/z* calcd for $C_{11}H_{12}N_2O_2S_2$ (M^+), 268.0340; found, 268.0330. Anal. ($C_{11}H_{12}N_2O_2S_2$) H, N; C: calcd, 49.23; found, 48.71.

5,6,7,8-Tetrahydro-7-methyl-2-(dimethylamino)-4*H*-pyrido[4′,3′:4,5]thieno[2,3-*d*][1,3]oxazin-4-one (37): General Procedure for Thieno[2,3-*d*][1,3]oxazin-4-ones 37, 38, and 40. Compound **29** (1.34 g, 5 mmol) was dissolved in dry $Cl(CH_2)_2Cl$ (70 mL), and dichloromethylene dimethylammonium chloride (0.81 g, 5 mmol) was added. After being stirred for 1 h at room temperature and 1 h at 50 °C, the reaction mixture was cooled to 0 °C, treated with 1 M ethereal HCl (6.1 mL), stirred for 1 h at 0 °C, and refluxed for 3.5 h. After cooling, the precipitate was collected by filtration, washed with cold $Cl(CH_2)_2Cl$, and dried. The crude product was dissolved in ice−water (650 mL) and filtered. The acidic filtrate (pH 3−4) was adjusted to pH 10 by dropwise addition of saturated aqueous Na_2CO_3 and extracted with ethyl acetate (1 × 250 mL and 2 × 500 mL). The organic layer was washed with H_2O (200 mL) and dried (Na_2SO_4). The solvent was removed in vacuo, and the residue was purified by column chromatography (petrol ether/CH_3COCH_3/CH_3OH, 5:3:2) to yield **37** (0.34 g, 26%) as yellowish crystals: mp 166−169 °C (decomp); HRMS *m/z* calcd for $C_{12}H_{15}N_3O_2S$ (M^+), 265.0885; found, 265.0887. Anal. ($C_{12}H_{15}N_3O_2S$) C, H; N: calcd, 15.84; found, 15.39.

7-Ethyl-5,6,7,8-tetrahydro-2-(dimethylamino)-4*H*-pyrido[4′,3′:4,5]thieno[2,3-*d*][1,3]oxazin-4-one (38). This compound was prepared from **30** (1.41 g, 5 mmol). The crude product was dissolved in ice−water (700 mL) and filtered. The acidic filtrate (pH 4) was adjusted to pH 10 by dropwise addition of saturated aqueous Na_2CO_3, and extracted with ethyl acetate (3 × 500 mL). The organic layer was washed with H_2O (200 mL) and dried (Na_2SO_4). The solvent was removed in vacuo, and the residue was purified by 2-fold column chromatography (petrol ether/CH_3COCH_3/CH_3OH, 5:3:2) and recrystallization from *n*-hexane to yield **38** (0.09 g, 6%) as yellowish crystals: mp 95−96.5 °C; HRMS *m/z* calcd for $C_{13}H_{17}N_3O_2S$ (M^+), 279.1041; found, 279.1039. Anal. ($C_{13}H_{17}N_3O_2S$ × 0.25 H_2O) C, H, N.

5,6,7,8-Tetrahydro-2-(dimethylamino)-7-(2-methylpropyl)-4*H*-pyrido[4′,3′:4,5]thieno[2,3-*d*][1,3]oxazin-4-one (39). Compound **31** (1.55 g, 5 mmol) was dissolved in dry $Cl(CH_2)_2Cl$ (70 mL), and dichloromethylene dimethylammonium chloride (0.81 g, 5 mmol) was added. After being stirred for 1 h at room temperature and 1 h at 50 °C, the reaction mixture was cooled to 0 °C, treated with 1 M ethereal HCl (6.1 mL), stirred for 1 h at 0 °C, and refluxed for 3.5 h. The solvent was removed in vacuo; the residue was dissolved in ice−water (700 mL) and filtered. The acidic filtrate (pH 4−5) was adjusted to pH 10 by dropwise addition of saturated aqueous Na_2CO_3 and extracted with ethyl acetate (2 × 250 mL and 2 × 500 mL). The organic layer was washed with H_2O (2 × 250 mL) and dried (Na_2SO_4). The solvent was removed in vacuo, and the residue was purified by column chromatography (ethyl acetate) and recrystallization from *n*-hexane to yield **39** (0.29 g, 19%) as yellow crystals: mp 117−118 °C; HRMS *m/z* calcd for $C_{15}H_{21}N_3O_2S$ (M^+), 307.1354; found, 307.1352. Anal. ($C_{15}H_{21}N_3O_2S$) H, N; C: calcd, 58.61; found, 59.06.

7-Benzyl-5,6,7,8-tetrahydro-2-(dimethylamino)-4*H*-pyrido[4′,3′:4,5]thieno[2,3-*d*][1,3]oxazin-4-one (40). This compound was prepared from **1** (1.72 g, 5 mmol). The crude product was dissolved in ice−water (800 mL) and filtered. The acidic filtrate (pH 3−4) was adjusted to pH 10 by dropwise addition of saturated sodium carbonate solution and extracted with ethyl acetate (2 × 200 mL and 2 × 300 mL). The organic layer was washed with H_2O (3 × 300 mL) and dried (Na_2SO_4). The solvent was removed in vacuo, and the residue was purified by column chromatography (petrol ether/ethyl acetate, 2:1) to yield **40** as yellowish crystals. A second fraction from the chromatographic purification was recrystallized from *n*-hexane to obtain an additional amount of the product (total yield 0.47 g, 28%): mp 147−148 °C; HRMS *m/z* calcd for $C_{18}H_{19}N_3O_2S$ (M^+), 341.1198; found, 341.1184. Anal. ($C_{18}H_{19}N_3O_2S$) C, H, N.

7-Benzoyl-5,6,7,8-tetrahydro-2-(dimethylamino)-4*H*-pyrido[4′,3′:4,5]thieno[2,3-*d*][1,3]oxazin-4-one (41). Compound **32** (1.08 g, 3 mmol) was dissolved in dry $Cl(CH_2)_2Cl$ (100 mL), and dichloromethylene dimethylammonium chloride (0.49 g, 3 mmol) was added. After being stirred for 1.5 h at room temperature and 1 h at 50 °C, the reaction mixture was cooled to 0 °C, treated with 1 M ethereal HCl (1.8 mL), stirred for 30 min at 0 °C, and refluxed for 3.5 h. After removal of the solvent in vacuo, the crude product was purified by column chromatography (ethyl acetate) to obtain **41** (0.30 g, 27%) as a yellowish solid: mp 159−162 °C (*n*-hexane, decomp); HRMS *m/z* calcd for $C_{18}H_{17}N_3O_3S$ (M^+), 355.0991; found, 355.0995. Anal. ($C_{18}H_{17}N_3O_3S$ × 0.5 H_2O) C, H, N.

Ethyl 6-Benzyl-4,5,6,7-tetrahydro-2-(3-isopropylthioureido)thieno[2,3-*c*]pyridine-3-carboxylate (44). A mixture of **42** (6.33 g, 20 mmol), isopropyl isothiocyanate (2.83 g, 28 mmol), and dry C_2H_5OH (8 mL) was stirred in an autoclave at 80 °C for 18 h under argon atmosphere. After cooling, further isopropyl isothiocyanate (2.83 g, 28 mmol) was added, and the reaction mixture was stirred at 80 °C for 23 h. After keeping at room-temperature overnight, the precipitate was collected by filtration, washed with cold C_2H_5OH, and dried to obtain **44** (7.13 g, 78%) as a salmon solid: mp 114.5−117 °C (CH_3OH). Anal. ($C_{21}H_{27}N_3O_2S_2$ × 1.2 CH_3OH) C, N; H: calcd, 7.03; found, 6.61.

2-Amino-7-benzyl-5,6,7,8-tetrahydro-4*H*-pyrido[4′,3′:4,5]thieno[2,3-*d*][1,3]thiazin-4-one (47). Compound **47** was prepared from **43** as described, mp 161−163 °C.[76]

7-Benzyl-5,6,7,8-tetrahydro-2-isopropylamino-4*H*-pyrido[4′,3′:4,5]thieno[2,3-*d*][1,3]-thiazin-4-one (48). A mixture of compound **44** (2.09 g, 5 mmol) and concentrated H_2SO_4

(10 mL) was kept at room temperature for 3 days and poured into a mixture of saturated aqueous $NaHCO_3$ (500 mL) and ice (500 g). The precipitate was collected by filtration, washed with H_2O, and dried to obtain **48** (1.67 g, 90%) as a yellow solid: mp 193.5−197 °C (CH_3OH, decomp); HRMS *m/z* calcd for $C_{19}H_{20}N_3OS_2$ ($M^+ - H$), 370.1048; found, 370.1041. Anal. ($C_{19}H_{21}N_3OS_2$) C, H, N.

7-Benzyl-2-cyclohexylamino-5,6,7,8-tetrahydro-4*H*-pyrido[4′,3′:4,5]thieno[2,3-*d*][1,3]thiazin-4-one (49). Compound **49** was prepared from **45** as described, mp 204−205 °C.[77]

7-Benzyl-5,6,7,8-tetrahydro-2-phenylamino-4*H*-pyrido-[4′,3′:4,5]thieno[2,3-*d*][1,3]thiazin-4-one (50). Compound **50** was prepared from **46** as described, mp 147−149 °C.[77]

2-Benzoylamino-7-benzyl-5,6,7,8-tetrahydro-4*H*-pyrido-[4′,3′:4,5]thieno[2,3-*d*][1,3]thiazin-4-one (51). A mixture of compound **43** (1.44 g, 3 mmol) and concentrated H_2SO_4 (6 mL) was kept at room temperature for 2 days and poured into ice−water (200 mL). The solution was adjusted to pH 8−9 by dropwise addition of 2.5 N aqueous NaOH (70 mL) and 5% aqueous Na_2CO_3 (2.5 mL). The precipitate was collected by filtration, washed with H_2O, dried, and recrystallized from ethyl acetate to obtain **51** (0.38 g, 29%) as yellow crystals: mp 217−220 °C (decomp); HRMS *m/z* calcd for $C_{23}H_{19}N_3O_2S_2$ (M^+), 433.0919; found, 433.0910. Anal. ($C_{23}H_{19}N_3O_2S_2$) C, H, N.

Kinetic Analysis of the Nonenzymatic Hydrolysis. Alkaline hydrolysis was followed spectrophotometrically at a fixed wavelength (thieno[1,3]oxazin-4-ones **4**, **5**, **7**, **8**, **12**, **19**−**23**, **33**−**41**, and **62** = 325−338 nm and thieno[1,3]thiazin-4-ones **47**−**51** = 367 nm), by monitoring the disappearance of the compounds in 50 mM CAPS, pH 11.0, at 25 °C. Stock solutions of the inhibitors were prepared in DMSO; the final inhibitor concentration was 2.5−20 μM and the final DMSO concentration was 5%. Curves were analyzed as first-order reactions.

CEase Inhibition Assay in the Presence of a Chromogenic Substrate. CEase inhibition was assayed spectrophotometrically at 25 °C.[30,94] Assay buffer was 100 mM sodium phosphate, 100 mM NaCl, pH 7.0. A stock solution of CEase (2.44 mg/mL) in 100 mM sodium phosphate buffer, pH 7.0, was 1:20 diluted with the same buffer and kept at 0 °C for 4 h. A 1:122 dilution was done immediately before starting the measurement. TC (12 mM) was dissolved in assay buffer and kept at 25 °C. Compounds **49** and **51** were dissolved in a 1:1 mixture of 0.1 M HCl and acetonitrile. Stock solutions of all other inhibitors and of pNPB (20 mM) were prepared in acetonitrile. Thieno[1,3]oxazin-4-ones **4**, **5**, **7**, **8**, **12**, **19**−**23**, **35**, **37**−**41**, **52**−**55**, and **59**−**63**, as well as thieno[1,3]thiazin-4-ones **47**−**51** were analyzed at a single concentration (5−50 μM). K_i values were calculated using the equation $K_i(1 + [S]/K_m^S) = [I]/(v_0/v - 1)$, where v_0 and v are the rates in the absence and presence of inhibitor. For thieno[1,3]oxazin-4-ones **33**, **34**, **36**, and **58**, at least five different inhibitor concentrations were used. Progress curves were characterized by a linear steady-state turnover of the substrate, and values of a linear regression were fitted to an equation of competitive inhibition to obtain $K_i(1 + [S]/K_m^S)$ values. Into a cuvette containing 430 μL of assay buffer, 500 μL of the TC solution, 40 μL of acetonitrile, 10 μL of the pNPB solution, and 10 μL of an inhibitor solution were added and thoroughly mixed. After incubation for 5 min at 25 °C, the reaction was initiated by adding 10 μL of the enzyme solution (1 μg/mL). Inhibition studies with the compounds **49** and **51** were performed under the same conditions, using 425 μL of buffer and 45 μL of acetonitrile. Concentrations were as follows: 200 μM pNPB ($1.82 \times K_m^S$),[35] 6 mM TC, 10 ng/mL CEase, 6% acetonitrile, and different inhibitor concentrations. Uninhibited enzyme activity was determined by adding acetonitrile instead of the inhibitor solution. The rates of CEase-catalyzed pNPB hydrolysis were corrected by those of the nonenzymatic hydrolysis of pNPB as determined by using 10 μL of 100 mM sodium phosphate buffer, pH 7.0, instead of the enzyme solution. Progress curves were monitored at 405 nm over 6 min. Similarly, the inhibition of CEase by compound **33** (4−12 μM) was studied in the presence of different substrate concentrations (100−600 μM).

CEase-Catalyzed Turnover of the Heterocyclic Compounds. The enzymatic conversion of the compounds was followed spectrophotometrically at 25 °C. Into a cuvette containing assay buffer, 500 μL of TC solution, 50 μL of acetonitrile, and 10 μL of an inhibitor solution were added, thoroughly mixed, and incubated for 5 min at 25 °C. The reaction was initiated by adding a volume (59.8−61.3 μL) of a CEase solution (122 μg/mL). This volume was adjusted by the determination of a 1:6250 dilution that converts pNPB (200 μM) with a rate of 18 μM/min. A molar extinction coefficient, $\epsilon = 7.67\ mM^{-1}\ cm^{-1}$, for *p*-nitrophenol at pH 7.0 was used for this purpose. The entire volume was 1 mL containing the following concentrations: 6 mM TC, CEase (adjusted activity), 6% acetonitrile, and 25 μM inhibitor. Reactions were analyzed by monitoring UV/vis spectra in fixed time intervals or by following the time course at 350 nm. The molar extinction coefficient at 350 nm for each analyzed compound was determined separately in duplicate experiments at 10 different concentrations (5−50 μM). Control experiments to prove the stability of the compounds were performed by adding 100 mM sodium phosphate buffer, pH 7.0, instead of the enzyme solution.

AChE Inhibition Assay. AChE inhibition was assayed spectrophometrically at 25 °C according to the method of Ellman et al.[95] Assay buffer was 100 mM sodium phosphate, 100 mM NaCl, pH 7.3. A stock solution of AChE (100 U/mL) in assay buffer was kept at 0 °C. A 1:30 dilution was prepared immediately before starting the measurement. ATCh (10 mM) and DTNB (7 mM) were dissolved in assay buffer and kept at 0 °C. Galanthamine, tacrine, and compounds **49** and **51** were dissolved in a 1:1 mixture of 0.1 M HCl and acetonitrile. Stock solutions of all other inhibitors were prepared in acetonitrile. Thieno[1,3]oxazin-4-ones **33**−**36** and **52**−**63**, as well as thieno-[1,3]thiazin-4-one **51** were analyzed at a single concentration (5−50 μM). IC_{50} values were calculated using the equation $IC_{50} = [I]/(v_0/v - 1)$, where v_0 and v are the rates in the absence and presence of inhibitor. For galanthamine, tacrine, and the thieno[1,3]oxazin-4-ones **4**, **5**, **7**, **8**, **12**, **19**−**23**, and **37**−**41**, as well as the thieno[1,3]thiazin-4-ones **47**−**50** at least five different inhibitor concentrations were used. Progress curves were characterized by a linear steady-state turnover of the substrate and values of a linear regression were fitted according to eq 1. Into a cuvette containing 830 μL of assay buffer, 50 μL of the DTNB solution, 50 μL of acetonitrile, 10 μL of an inhibitor solution, and 10 μL of an AChE solution (3.33 U/ml) were added and thoroughly mixed. After incubation for 15 min at 25 °C, the reaction was initiated by adding 50 μL of the ATCh solution. Inhibition studies with galanthamine, tacrine, and compounds **49** and **51** were performed under the same conditions, using 825 μL of buffer and 55 μL of acetonitrile. Concentrations were as follows: 500 μM ATCh ($0.91 \times K_m$), 350 μM DTNB, 0.033 U/mL AChE, 6% acetonitrile, and different inhibitor concentrations. Uninhibited enzyme activity was determined by adding acetonitrile instead of the inhibitor solution. Determination of Michaelis constant for the substrate ATCh was done at 11 different ATCh concentrations (50−2500 μM) to give a value $K_m = 550 \pm 40$ μM. The rates of AChE-catalyzed ATCh hydrolysis were corrected by those of the nonenzymatic hydrolysis of ATCh as determined by using 10 μL of assay buffer, instead of the enzyme solution. Progress curves were monitored at 412 nm over 5 min. Similarly, the inhibition of AChE by galanthamine (0.76−8 μM), tacrine (0.02−0.1 μM), **39** (1−6 μM), and **40** (2−6 μM) was studied in the presence of different substrate concentrations (250−1000 μM).

Acknowledgment. The authors thank C. M. González Tanarro for analyzing AChE inhibition by galanthamine and tacrine and are grateful to the Graduate College 677 for financial support.

Supporting Information Available: Kinetic analysis of the inhibition of CEase, elemental analysis data, IR data, UV data, ^{1}H NMR data, ^{13}C NMR data, and MS (EI) data of the synthesized compounds. This material is available free of charge via the Internet at http://pubs.acs.org.

References

(1) Cygler, M.; Schrag, J. D.; Sussman, J. L.; Harel, M.; Silman, I.; Gentry, M. K.; Doctor, B. P. Relationship between sequence conservation and three-dimensional structure in a large family of esterases, lipases, and related proteins. *Protein Sci.* **1993**, *2*, 366−382.

(2) Nardini, M.; Dijkstra, B. W. α/β Hydrolase fold enzymes: the family keeps growing. *Curr. Opin. Struct. Biol*. **1999**, *9*, 732−737.

(3) Ollis, D. L.; Cheah, E.; Cygler, M.; Dijkstra, B.; Frolow, F.; Franken, S. M.; Harel, M.; Reington, S. J.; Silman, I.; Schrag, J.; Sussman, J. L.; Verschueren, K. H. G.; Goldman, A. The α/β hydrolase fold. *Protein Eng*. **1992**, *5*, 197−211.

(4) Holmquist, M. Alpha/beta-hydrolase fold enzymes: structures, functions and mechanisms. *Curr. Protein Pept. Sci.* **2000**, *1*, 209−235.

(5) Heikinheimo, P.; Goldman, A.; Jeffries, C.; Ollis, D. L. Of barn owls and bankers: a lush variety of α/β hydrolases. *Structure* **1999**, *7*, R141−R146.

(6) Quinn, D. M.; Feaster, S. R. Esterases and lipases. In *Comprehensive biological catalysis. A mechanistic reference*; Sinnot, M., Ed.; Academic Press: San Diego, 1998; Volume I, pp 455−482.

(7) Lin, G.; Li, Y.-R.; Liu, Y.-C.; Wu, Y.-G. *Ortho* effects for inhibition mechanisms of butyrylcholinesterase by *o*-substituted phenyl *N*-butyl carbamates and comparison with acetylcholinesterase, cholesterol esterase, and lipase. *Chem. Res. Toxicol.* **2005**, *18*, 1124−1131.

(8) Wang, X.; Wang, C.-S.; Tang, J.; Dyda, F.; Zhang, X. C. The crystal structure of bovine bile salt activated lipase: insights into the bile salt activation mechanism. *Structure* **1997**, *5*, 1209−1218.

(9) Chen, J. C.-H.; Miercke, L. J. W.; Krucinski, J.; Starr, J. R.; Saenz, G.; Wang, X.; Spilburg, C. A.; Lange, L. G.; Ellsworth, J. L.; Stroud, R. M. Structure of bovine pancreatic cholesterol esterase at 1.6 Å: novel structural features involved in lipase activation. *Biochemistry* **1998**, *37*, 5107−5117.

(10) Terzyan, S.; Wang, C.-S.; Downs, D.; Hunter, B.; Zhang, X. C. Crystal structure of the catalytic domain of human bile salt activated lipase. *Protein Sci.* **2000**, *9*, 1783−1790.

(11) Moore, S. A.; Kingston, R. L.; Loomes, K. M.; Hernell, O.; Bläckberg, L.; Baker, H. M.; Baker, E. N. The structure of truncated recombinant human bile salt-stimulated lipase reveals bile salt-independet conformational flexibility at the active-site loop and provides insights into heparin binding. *J. Mol. Biol.* **2001**, *312*, 511−523.

(12) Rudd, E. A.; Brockmann, H. L. Pancreatic carboxyl ester lipase (cholesterol esterase). In *Lipases*; Borgstrom, B., Brockmann, H. L., Eds.; Elsevier Science: New York, 1984; pp 185−204.

(13) Lombardo, D.; Fauvel, J.; Guy, O. Studies on the substrate specificity of a carboxyl ester hydrolase from human pancreatic juice. I. Action on carboxyl esters, glycerides and phospholipids. *Biochim. Biophys. Acta* **1980**, *611*, 136−146.

(14) Lombardo, D.; Guy, O. Studies on the substrate specificity of a carboxyl ester hydrolase from human pancreatic juice. II. Action on cholesterol esters and lipid-soluble vitamin esters. *Biochim. Biophys. Acta* **1980**, *611*, 147−155.

(15) Hui, D. Y. Molecular biology of enzymes involved with cholesterol ester hydrolysis in mammalian tissues. *Biochim. Biophys. Acta* **1996**, *1303*, 1−14.

(16) Hui, D. Y.; Howles, P. N. Carboxyl ester lipase: structure−function relationship and physiological role in lipoprotein metabolism and atherosclerosis. *J. Lipid Res.* **2002**, *43*, 2017−2030.

(17) Heidrich, J. E.; Contos, L. M.; Hunsaker, L. A.; Deck, L. M.; Vander Jagt, D. L. Inhibition of pancreatic cholesterol esterase reduces cholesterol absorption in the hamster. *BMC Pharmacol.* **2004**, *4*:5.

(18) Ikeda, I.; Matsuoka, R.; Hamada, T.; Mitsui, K.; Imabayashi, S.; Uchino, A.; Sato, M.; Kuwano, E.; Itamura, T.; Yamada, K.; Tanaka, K.; Imaizumi, K. Cholesterol esterase accelerates intestinal cholesterol absorption. *Biochim. Biophys. Acta* **2002**, *1571*, 34−44.

(19) Myers-Payne, S. C.; Hui, D. Y.; Brockman, H. L.; Schroeder, F. Cholesterol esterase: a cholesterol transfer protein. *Biochemistry* **1995**, *34*, 3942−3947.

(20) Brodt-Eppley, J.; White, P.; Jenkins, S.; Hui, D. Y. Plasma cholesterol esterase level is a determinant for an atherogenic lipoprotein profile in normolipidemic human subjects. *Biochim. Biophys. Acta* **1995**, *1272*, 69−72.

(21) Chao, F.-F.; Blanchette-Mackie, E. J.; Tertov, V. V.; Skarlatos, S. I.; Chen, Y. J.; Kruth, H. S. Hydrolysis of cholesteryl ester in low density lipoprotein converts this lipoprotein into a liposome. *J. Biol. Chem.* **1992**, *267*, 4992−4998.

(22) Chao, F.-F.; Blanchette-Mackie, E. J.; Chen, Y. J.; Dickens, B. F.; Berlin, E.; Amende, L. M.; Skarlatos, S. I.; Gamble, W.; Resau, J. H.; Mergner, W. T.; Kruth, H. S. Characterization of two unique cholesterol-rich lipid particles isolated from human atherosclerotic lesions. *Am. J. Pathol.* **1990**, *136*, 169−179.

(23) Chao, F.-F.; Amende, L. M.; Blanchette-Mackie, E. J.; Skarlatos, S. I.; Gamble, W.; Resau, J. H.; Mergner, W. T.; Kruth, H. S. Unesterified cholesterol-rich lipid particles in atherosclerotic lesions of human and rabbit aortas. *Am. J. Pathol.* **1988**, *131*, 73−83.

(24) Guarino, A. J.; Tulenko, T. N.; Wrenn, S. P. Cholesterol crystal nucleation from enzymatically modified low-density lipoproteins: combined effect of sphingomyelinase and cholesterol esterase. *Biochemistry* **2004**, *43*, 1685−1693.

(25) Li, F.; Huang, Y.; Hui, D. Y. Bile salt stimulated cholesterol esterase increases uptake of high-density lipoprotein-associated cholesteryl esters by HepG2 cells. *Biochemistry* **1996**, *35*, 6657−6663.

(26) Shamir, R. W.; Johnson, J.; Morlock-Fitzpatrick, K.; Zolfaghari, R.; Li, L.; Mas, E.; Lombardo, D.; Morel, D. W.; Fisher, E. A. Pancreatic carboxyl ester lipase: a circulating enzyme that modifies normal and oxidized lipoproteins *in vitro*. *J. Clin. Invest.* **1996**, *97*, 1696−1704.

(27) Li, F.; Hui, D. Y. Synthesis and secretion of the pancreatic-type carboxyl ester lipase by human endothelial cells. *Biochem. J.* **1998**, *329*, 675−679.

(28) Augé, N.; Nikolova-Karakashian, M.; Carpentier, S.; Parthasarathy, S.; Nègre Salvayre, A.; Salvayre, R.; Merrill, A. H., Jr.; Levade, T. Role of sphingosine 1-phosphate in the mitogenesis induced by oxidized low-density lipoprotein in smooth muscle cells *via* activation of sphingomyelinase, ceramidase, and sphingosine kinase. *J. Biol. Chem.* **1999**, *274*, 21533−21538.

(29) Feaster, S. R.; Quinn, D. M. Mechanism-based inhibitors of mammalian cholesterol esterase. *Methods Enzymol.* **1997**, *286*, 231−252.

(30) Feaster, S. R.; Lee, K.; Baker, N.; Hui, D. Y.; Quinn, D. M. Molecular recognition by cholesterol esterase of active site ligands: structure−reactivity effects for inhibition by aryl carbamates and subsequent carbamylenzyme turnover. *Biochemistry* **1996**, *35*, 16723−16734.

(31) Lin, G.; Shieh, C.-T.; Ho, H.-C.; Chouhwang, J.-Y.; Lin, W.-Y.; Lu, C.-P. Structure−reactivity relationships for the inhibition mechanism at the second alkyl-chain-binding site of cholesterol esterase and lipase. *Biochemistry* **1999**, *38*, 9971−9981.

(32) Lin, G.; Shieh, C.-T.; Tsai, Y.-C.; Hwang, C.-I.; Lu, C.-P.; Cheng, G.-H. Structure−reactivity probes for active site shapes of cholesterol esterase by carbamate inhibitors *Biochim. Biophys. Acta* **1999**, *1431*, 500−511.

(33) Deck, L. M.; Baca, M. L.; Salas, S. L.; Hunsacker, L. A.; Vander Jagt, D. L. 3-Alkyl-6-chloro-2-pyrones: selective inhibitors of pancreatic cholesterol esterase. *J. Med. Chem.* **1999**, *42*, 4250−4256.

(34) Stoddard Hatch, M.; Brown, W. M.; Deck, J. A.; Hunsaker, L. A.; Deck, L. M.; Vander Jagt, D. L. Inhibition of yeast lipase (CRL1) and cholesterol esterase (CRL3) by 6-chloro-2-pyrones: comparison with porcine cholesterol esterase. *Biochim. Biophys. Acta* **2002**, *1596*, 381−391.

(35) Pietsch, M.; Gütschow, M. Alternate substrate inhibition of cholesterol esterase by thieno[2,3-*d*][1,3]oxazin-4-ones. *J. Biol. Chem.* **2002**, *277*, 24006−24013.

(36) Krantz, A.; Spencer, R. W.; Tam, T. F.; Liak, T. J.; Copp, L. J.; Thomas, E. M.; Rafferty, S. P. Design and synthesis of 4*H*-3,1-benzoxazin-4-ones as potent alternate substrate inhibitors of human leukocyte elastase. *J. Med. Chem*. **1990**, *33*, 464−479.

(37) Stein, R. L.; Strimpler, A. M.; Viscarello, B. R.; Wildonger, R. A.; Mauger, R. C.; Trainor, D. A. Mechanism for slow-binding inhibition of human leukocyte elastase by valine-derived benzoxazinones. *Biochemistry* **1987**, *26*, 4126−4130.

(38) Gütschow, M.; Neumann, U. Novel thieno[2,3-*d*][1,3]oxazin-4-ones as inhibitors of human leukocyte elastase. *J. Med. Chem*. **1998**, *41*, 1729−1740.

(39) Gütschow, M.; Kuerschner, L.; Neumann, U.; Pietsch, M.; Löser, R.; Koglin, N.; Eger, K. 2-(Diethylamino)thieno[1,3]oxazin-4-ones as stable inhibitors of human leukocyte elastase. *J. Med. Chem*. **1999**, *42*, 5437−5447.

(40) Neumann, U.; Schechter, N. M.; Gütschow, M. Inhibition of human chymase by 2-amino-3,1-benzoxazin-4-ones. *Bioorg. Med. Chem*. **2001**, *9*, 945−954.

(41) Gütschow, M.; Kuerschner, L.; Pietsch, M.; Ambrożak, A.; Neumann, U.; Günther, R.; Hofmann, H.-J. Inhibition of cathepsin G by 2-amino-3,1-benzoxazin-4-ones: kinetic investigations and docking studies. *Arch. Biochem. Biophys.* **2002**, *402*, 180−191.
(42) Zschörnig, O.; Pietsch, M.; Süss, R.; Schiller, J.; Gütschow, M. Cholesterol esterase action on human high-density lipoproteins and inhibition studies: detection by MALDI-TOF MS. *J. Lipid Res.* **2005**, *46*, 803−811.
(43) Soreq, H.; Seidman, S. Acetylcholinesterase − new roles for an old actor. *Nat. Rev. Neurosci.* **2001**, *2*, 294−302.
(44) Quinn, D. M. Acetylcholinesterase: enzyme structure, reaction dynamics, and virtual transition states. *Chem. Rev.* **1987**, *87*, 955−979.
(45) Massoulié, J. The origin of the molecular diversity and functional anchoring of cholinesterases. *Neurosignals* **2002**, *11*, 130−143.
(46) Silman, I.; Sussman, J. L. Acetylcholinesterase: 'classical' and 'nonclassical' functions and pharmacology. *Curr. Opin. Pharmacol.* **2005**, *5*, 293−302.
(47) Layer P. G.; Weikert, T.; Alber, R. Cholinesterases regulate neurite growth of chick nerve cells *in vitro* by means of a non-enzymatic mechanism. *Cell Tissue Res.* **1993**, *273*, 219−226.
(48) Grisaru, D.; Sternfeld, M.; Eldor, A.; Glick, D.; Soreq, H. Structural roles of acetylcholinesterase variants in biology and pathology. *Eur. J. Biochem.* **1999**, *264*, 672−686.
(49) Bartolini, M.; Bertucci, C.; Cavrini, V.; Andrisano, V. Beta-amyloid aggregation induced by human acetylcholinesterase: inhibition studies. *Biochem. Pharmacol.* **2003**, *65*, 407−416.
(50) Alvarez, A.; Opazo, C.; Alarcon, R.; Garrido, J.; Inestrosa, N. C. Acetylcholinesterase promotes the aggregation of amyloid-beta-peptide fragments by forming a complex with the growing fibrils. *J. Mol. Biol.* **1997**, *272*, 348−361.
(51) Rees, T.; Hammond, P. I.; Soreq, H.; Younkin, S.; Brimijoin, S. Acetylcholinesterase promotes beta-amyloid plaques in cerebral cortex. *Neurobiol. Aging* **2003**, *24*, 777−787.
(52) Chacón, M. A.; Reyes; A. E.; Inestrosa, N. C. Acetylcholinesterase induces neuronal cell loss, astrocyte hypertrophy and behavioral deficits in mammalian hippocampus. *J. Neurochem.* **2003**, *87*, 195−204.
(53) Alvarez, A.; Alarcon, R.; Opazo, C.; Campos, E. O.; Munoz, F. J.; Calderon, F. H.; Dajas, F.; Gentry, M. K.; Doctor, B. P.; De Mello, F. G.; Inestrosa, N. C. Stable complexes involving acetylcholinesterase and amyloid-beta peptide change the biochemical properties of the enzyme and increase the neurotoxicity of Alzheimer's fibrils. *J. Neurosci.* **1998**, *18*, 3213−3223.
(54) Reyes, A. E.; Chacón, M. A.; Dinamarca, M. C.; Cerpa, W.; Morgan, C.; Inestrosa, N. C. Acetylcholinesterase-Aβ complexes are more toxic than Aβ fibrils in rat hippocampus. *Am. J. Pathol.* **2004**, *164*, 2163-2174.
(55) Carson, K. A.; Geula, C.; Mesulam, M.-M. Electron microscopic localization of cholinesterase activity in Alzheimer brain tissue. *Brain Res.* **1991**, *540*, 204−208.
(56) Wright, C. I.; Geula, C.; Mesulam, M.-M. Protease inhibitors and indoleamines selectively inhibit cholinesterases in the histopathologic structures of Alzheimer disease. *Proc. Natl. Acad. Sci. U.S.A.* **1993**, *90*, 686−686.
(57) Inestrosa, N. C.; Alarcon, R. Molecular interactions of acetylcholinesterase with senile plaques. *J. Physiol. (Paris)* **1998**, *92*, 341−344.
(58) Selkoe, D. J. Alzheimer's disease: genes, proteines, and therapy. *Phys. Rev.* **2001**, *81*, 741−766.
(59) Inestrosa, N. C.; Sagal, J. P.; Colombres, M. Acetylcholinesterase interactions with Alzheimer amyloid β. *Subcell Biochem.* **2005**, *38*, 299−317.
(60) Recanatini, M.; Valenti, P. Acetylcholinesterase inhibitors as a starting point towards improved Alzheimer's disease therapeutics. *Curr. Pharm. Des.* **2004**, *10*, 3157−3166.
(61) Benzi, G.; Moretti, A. Is there a rationale for the use of acetylcholinesterase inhibitors in the therapy of Alzheimer's disease? *Eur. J. Pharmacol.* **1998**, *346*, 1−13.
(62) Colombres, M.; Sagal, J. P.; Inestrosa, N. C. An overview of the current and novel drugs for Alzheimer's disease with particular reference to anti-cholinesterase compounds. *Curr. Pharm. Des.* **2004**, *10*, 3121−3130.
(63) Rees, T. M.; Brimijoin, S. the role of acetylcholinesterase in the pathogenesis of Alzheimer's disease. *Drugs Today (Barc)* **2003**, *39*, 75−83.
(64) Ibach, B.; Haen, E. Acetylcholinesterase inhibition in Alzheimer's disease. *Curr. Pharm. Des.* **2004**, *10*, 231−251.
(65) Muñoz-Muriedas, J.; Lopez, J. M.; Orozco, M.; Luque, F. J. Molecular modelling approaches to the design of acetylcholinesterase inhibitors: new challenges for the treatment of Alzheimer's disease. *Curr. Pharm. Des.* **2004**, *10*, 3131−3140.
(66) Inestrosa, N. C.; Alvarez, A.; Perez, C. A.; Moreno R. D.; Vicente, M.; Linker, C.; Casanueva, O. I.; Soto, C.; Garrido, J. Acetylcholinesterase accelerates assembly of amyloid-beta-peptides into Alzheimer's fibrils: possible role of the peripheral site of the enzyme. *Neuron* **1996**, *16*, 881−891.
(67) Reyes, A. E.; Perez, D. R.; Alvarez, A. Garrido, J.; Gentry, M. K.; Doctor, B. P.; Inestrosa, N. C. A monoclonal antibody against acetylcholinesterase inhibits the formations of amyloid fibrils induced by the enzyme. *Biochem. Biophys. Res. Commun.* **1997**, *232*, 652−655.
(68) Sussman, J. L.; Harel, M.; Frolow, F.; Oefner, C.; Goldman, A.; Toker, L.; Silman, I. Atomic structure of acetylcholinesterase from *Torpedo californica*: a prototypic acetylcholine-binding protein. *Science* **1991**, *253*, 872−879.
(69) Harel, M.; Schalk, I.; Ehret-Sabatier, L.; Bouet, F.; Goeldner, M.; Hirth, C.; Axelsen, P. H.; Silman, I.; Sussman, J. L. Quaternary ligand binding to aromatic residues in the active-site gorge of acetylcholinesterase. *Proc. Natl. Acad. Sci. U.S.A.* **1993**, *90*, 9031−9035.
(70) Lin, G.; Chen, G.-H.; Yeh, S.-C.; Lu, C.-P. Probing the peripheral anionic site of acetycholinesterase with quantitative structure activity relationships for inhibition by biphenyl-4-acyoxylate-4′-*N*-butylcarbamates. *J. Biochem. Mol. Toxicol.* **2005**, *19*, 234−243.
(71) Piazzi, L.; Rampa, A.; Bisi, A.; Gobbi, S.; Belluti, F.; Cavalli, A.; Bartolini, M.; Andrisano, V.; Valenti, P.; Recanatini, M. 3-(4-{[Benzyl(methyl)amino]methyl}phenyl)-6,7-dimethoxy-2*H*-2-chromenone (AP2238) inhibits both acetylcholinesterase and acetylcholinesterase-induced β-amyloid aggregation: a dual function lead for Alzheimer's disease therapy. *J. Med. Chem.* **2003**, *46*, 2279−2282.
(72) Gewald, K.; Schinke, E.; Böttcher, H. 2-Aminothiophenes from methylene-active nitriles, carbonyl compounds, and sulfur. *Chem. Ber.* **1966**, *99*, 94−100.
(73) Sabnis, R. W. The Gewald synthesis. *Sulfur Rep.* **1994**, *16*, 1−17.
(74) Hallenbach, W.; Lindel, H.; Berschauer, F.; Scheer, M.; de Jong, A. Aminothienooxazinones as animal growth promotors. Ger. Offen. DE 3,540,377; *Chem. Abstr.* **1987**, *107*, 77818h.
(75) Player, M. R.; Sowell, J. W., Sr. Preparation of fused 1,3-oxazine-2,4-diones as potential antitumor agents. *J. Heterocycl. Chem.* **1995**, *32*, 1537−1540.
(76) Leistner, S.; Gütschow, M.; Wagner, G.; Grupe, R.; Böhme, B. One-step synthesis of 2-aminothieno[2,3-*d*][1,3]thiazin-4-ones in some cases 5,6-anellated from ethyl 2-benzoylthioureidothiophene-3-carboxylates and evaluation of their anti-allergy activity. *Pharmazie* **1988**, *43*, 466−470.
(77) Leistner, S.; Gütschow, M.; Wagner, G. The facile synthesis of 2-aminothieno[2,3-*d*][1,3]thiazin-4-ones, in some cases 5,6-anellated. *Synthesis* **1987**, *5*, 466−470.
(78) Hegarty, A. F.; Bruice, T. C. Acyl transfer reactions from and to the ureido functional group. I. The mechanisms of hydrolysis of an O-acylisourea (2-amino-4,5-benzo-6-oxo-1,3-oxazine. *J. Am. Chem.* Soc. **1970**, *92*, 6561−6567.
(79) Neumann, U.; Gütschow, M. 3,1-Benzothiazin-4-ones and 3,1-benzoxazin-4-ones: highly different activities in chymotrypsin inactivation. *Bioorg. Chem.* **1995**, *23*, 72−88.
(80) Segel, I. H. *Enzyme kinetics*; Wiley and Sons: New York, 1993; pp 161−226.
(81) Baici, A. The specific velocity plot. A graphical method for determining inhibition parameters for both linear and hyperbolic enzyme inhibitors. *Eur. J. Biochem.* **1981**, *119*, 9−14.
(82) Cornish-Bowden, A. *Fundamentals of enzyme kinetics*, 3rd ed.; Portland Press: London, 2004; pp 113−144.
(83) Wilkinson, G. N. Statistical estimations in enzyme kinetics. *Biochem. J.* **1961**, *80*, 324−332.
(84) Dowd, J. E.; Riggs, D. S. A comparison of estimates of Michaelis−Menten kinetic constants from various linear transformations. *J. Biol. Chem.* **1965**, *240*, 863−869.
(85) Nochi, S.; Asakawa, N.; Sato, T. Kinetic study on the inhibition of acetylcholinesterase by 1-benzyl-4-[(5,6-dimethoxy-1-indanon)-2-yl]methylpiperidine hydrochloride (E2020). *Biol. Pharm. Bull.* **1995**, *18*, 1145−1147.
(86) Brühlmann, C.; Marston, M.; Hostettmann, K.; Carrupt, P.-A.; Testa, B. Screening of non-alkaloidal natural compounds as acetylcholinesterase inhibitors. *Chem. Biodivers.* **2004**, *1*, 819−829.
(87) Greenblatt, H. M.; Kryger, G.; Lewis, T.; Silman, I.; Sussman, J. L. Structure of acetylcholinesterase complexed with (−)-galanthamine at 2.3 Å resolution. *FEBS Lett.* **1999**, *463*, 321−326.
(88) Bartolucci, C.; Perola, E.; Pilger, C.; Fels, G.; Lamba, D. Three-dimensional structure of a complex of galanthamine (Nivalin) with acetylcholinesterase from *Torpedo californica*: implications for the design of new anti-Alzheimer drugs. *Proteins* **2001**, *42*, 182−191.
(89) Doucet-Personeni, C.; Bentley, P. D.; Fletcher, R. J.; Kinkaid, A.; Kryger, G.; Pirard, B.; Taylor, A.; Taylor, R.; Taylor, J.; Viner, R.; Silman, I.; Sussman, J. L.; Greenblatt, H. M.; Lewis, T. A structure-based design approach to the development of novel, reversible AChE inhibitors. *J. Med. Chem.* **2001**, *44*, 3203−3215.

(90) Kryger, G.; Silman, I.; Sussman, J. L. Structure of acetylcholinesterase complexed with E2020 (Aricept): implications for the design of new anti-Alzheimer drugs. *Structure Fold. Des.* **1999**, *7*, 297−307.
(91) Nakanishi, M.; Tahara, T.; Nakatsu, O.; Imamura, H.; Maruyama, Y. 3,6-Disubstituted-4,5,6,7-tetrahydrothieno[2,3-*c*]pyridines. Ger. Offen. DE 1,812,404; *Chem. Abstr.* **1969**, *71*, 124402t.
(92) Julia, S.; Torrent, J.; Olle, J.; Ramio, J.; Sanz, M. Synthesis of 2-cyano-2-alkylethanols and their resolution through gas−liquid chromatography. *Afinidad* **1974**, *31*, 117−123.
(93) Baty, J. D.; Jones, Gurnos; Moore, C. 9-Aza steroids. III. Synthesis of some 2-cyclo-pentylquinolines as models for rings A, B, and D. *J. Org. Chem.* **1969**, *34*, 3295−3302.
(94) Hosie, L.; Sutton, L. D.; Quinn, D. M. *p*-Nitrophenyl and cholesteryl-*N*-alkyl carbamates as inhibitors of cholesterol esterase. *J. Biol. Chem.* **1987**, *262*, 260−264.
(95) Ellman, G. L.; Courtney, K. D.; Andres, V.; Featherstone, R. M. A new rapid colorimetric determination of acetylcholinesterase activity. *Biochem. Pharmacol.* **1961**, *7*, 88−95.

JM0508639